Anisotropy of Meteorological Fields[1]

Oleg A. Alduchov[2] Vladimir A. Gordin[3]

If we consider meteorological field as representations of stochastic (scalar and vector, with 3D argument) fields, the first moments – climate fields - include most essential information about the fields. But the second moments – correlation functions (CFs) – give some additional information about meteorological fields. Adequate CFs are necessary for many task with meteorological fields assimilation. This is a reason why CFs as well as their Fourier images - spectral densities - are investigated during last century, see [2] for details.

We have estimated, [1], the matrix-valued 3D CFs of geopotential height, temperature, and horizontal wind using most full global aerological dataset CARDS (Comprehensive Aerological Reference Data Set), 1948-2001 of radiosonde observations under homogeneity and isotropy hypotheses.

There is a strong mathematical problem here: to provide a positive definiteness of the approximated CFs. We solve the problem as a variational one using perturbation theory of Hermitian operators, [1,2]. We estimate the CFs for various months and geographical zones. The homogeneity and isotropy hypotheses were used here.

However the isotropy hypothesis is not strongly adequate especially is tropical zone – in [3-4] it has demonstrated, for separate points, but not for CF. Estimations on the base of 38-year observed data shows that anisotropy coefficients (relation of distance to equal correlations along of X-axis to Y-axis) are significantly above 1.0 for tropical zone (see Fig. 1-2). One have keep in the mind that number of observation is remarkable low for Southern hemisphere with respect to the Northern one. It is a reason for smoother estimations at Northern hemisphere.

To provide more adequate hypothesis we suppose to introduce a new Riemann metric for horizontal coordinates:

$$ds^2 = a(y,p)\cdot dx^2 + b(y,p)\cdot dx\cdot dy + c(y,p)\cdot dy^2, \quad \text{where } a,c>0,\ ac - b^2/4 > 0$$

and assume that CFs are isotropic in the new metrics.

Next step is to optimize the tensor's coefficients a,b,c according to our observational data. As a result we will get universal metric for description of anisotropic correlations.

References

1. O.A.Alduchov, V.A.Gordin. 3-D Correlation Functions of Basic Upper-Air Parameters. Izvestia of Russian Academy of Sciences. ser. ``The Physics of Atmosphere and Ocean", 2001, v.37, N1, pp.3-23 (Russian), 1-20 (English).
2. Gordin V.A.: Mathematical Problems and Methods in Hydrodynamic Weather Forecasting. Gordon & Breach Publ. House, 2000, 842p.
3. Hollingworth A., Lönnberg P.: The statistical structure of short-range forecast errors as determined from radiosonde data. Part I: The wind field. Tellus, 1986, 38A, p.111-136.
4. Lönnberg P., Hollingworth A.: The statistical structure of short-range forecast errors as determined from radiosonde data. Part II: The covariance of height and wind errors. Tellus, 1986, 38A, p.137-161.

---

[1] The work was partly supported by the grant 01-05-64748a;

[2] *Corresponding author address*: Dr. Oleg A. Alduchov, RIHMI-WDC, Korolev St., 6, Obninsk, Russia, 249020. E-mail: aoa@meteo.ru. *Research Institute of Hydrometeorological Information-World Data Center, Obninsk*

[3] *Corresponding author address*: Prof. Vladimir A. Gordin, Hydrometeorological Center of Russia, Bolshoi Predtechenskii per. 9-13, Moscow, 123376, Russia, E-mail: vagordin@vagordin.mccme.ru, vagordin@mail.ru. *Hydrometeorological Center of Russia, Moscow*

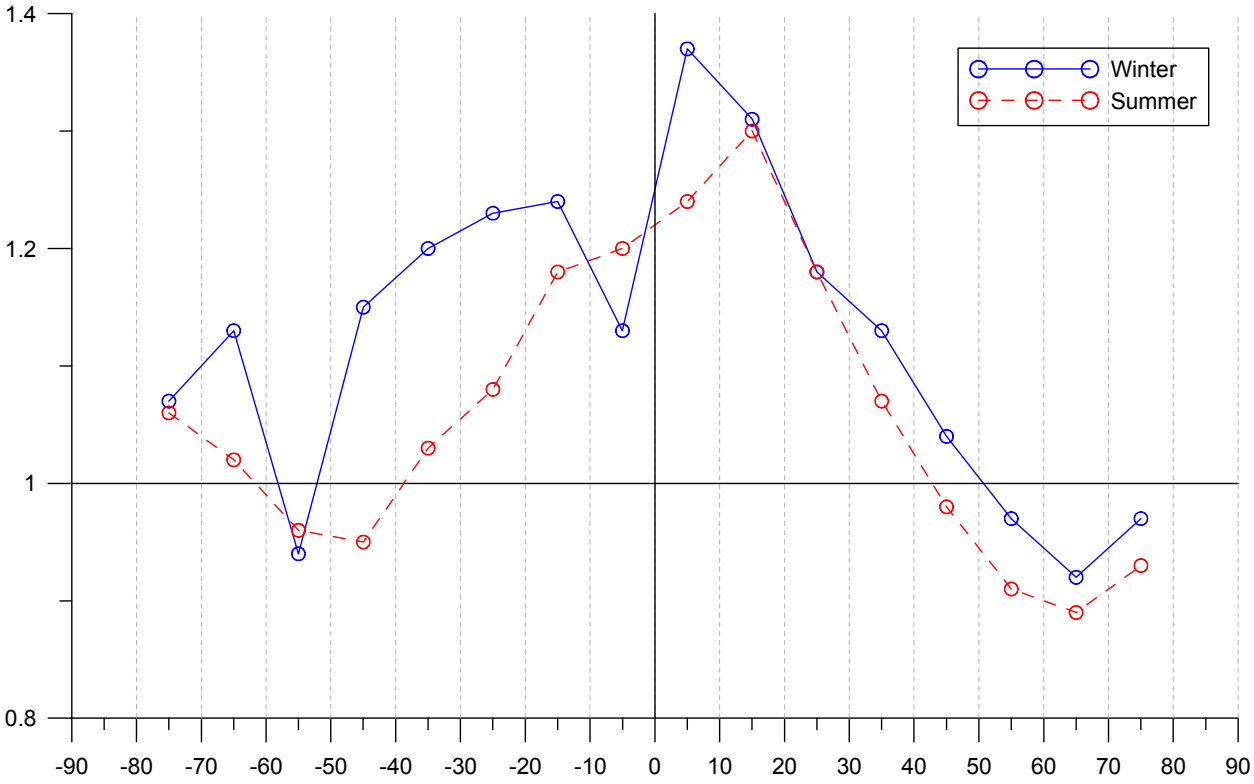

Figure1. Estimation of anisotropy coefficient for temperature at level 500 hPa.

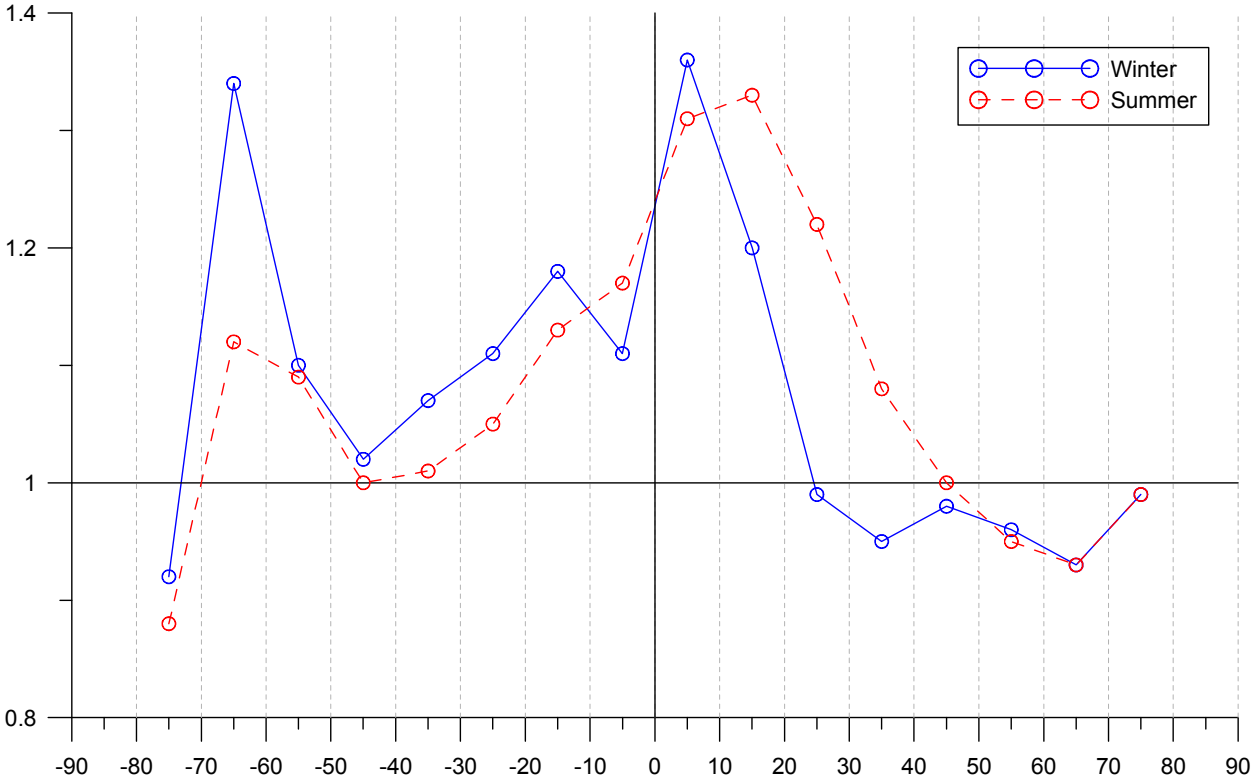

Figure 2. Estimation of anisotropy coefficient for geopotential height at level 500 hPa.

Errors in detecting of cloud boundaries for detailed radiosonde profiles

Oleg A. Alduchov (aoa@meteo.ru), Irina V. Chernykh (civ@meteo.ru),
Russian Institute of Hydrometeorological Information – Word Data Center, Obninsk, Russia
and Robert E. Eskridge (Beskridg@wmconnect.com), Asheville, USA

Last time new detailed upper-air soundings (for example, GPS sounding) with up to several hundred/thousands of observed levels and a distance between levels about 1-3 meters are used for determination of cloud boundaries [Chernykh and Alduchov, 2000; Naud, 2003] by CE-method [Chernykh and Eskridge, 1996; Chernykh et al. 2001].

The main goal of this paper is to pay special attention that detailed profiles may create a problem for various models on the base of derivatives estimations for upper-air variables.

For the very first look such soundings give much better understanding of the observed value profile, including gradient values, comparing to the standard upper-air soundings with 30-80 reported levels. But such detailed profile may create a problem for researcher, because of the current practice of reported values rounding.

Upper air report contains temperature values, rounded to the 0.1 °C, and relative humidity values, rounded to the 0.1%. It is easy to see, the upper estimate for the error of the gradient calculation using two nearest observed temperature values with a current rounding errors for resolution Δh of the profile is

$$\Delta T' = \frac{0.1}{\Delta h}$$

Hence, if $\Delta h = 1\,\text{m}$ (current GPS profiles), then the error of the temperature gradient due to rounding of temperature values is about 0.1 °C/m. Let's compare that value to the standard temperature gradient 0.7 °C per 100 m, i.e. 0.007 °C/m. The error is more than 14 times larger that the gradient itself – 1400% error. It is not acceptable for any task. In the same time, if resolution Δh of the profile is about 100 m, then the error due to rounding is about 0.001 °C/m, what means about 14% of the standard gradient, and it is almost acceptable for many tasks.

It means that for current accuracy of the temperature values in 0.1 °C the resolution of the vertical profile (for any tasks with gradient calculations) should be not less than 100-200 m or even more (what gives the error 14-7%, correspondently, because of the original values rounding for standard temperature gradient).

The problem looks even more serious if anybody will use standard observational errors at every reported height. For example, for the US radiosondes at current time the accuracy of temperature measurements is 0.5 °C from the surface to 20 hPa (and up to 1.0 °C at historical time series (see, Hawson, 1970, Hooper, 1978). But in reality an observational errors are significantly correlates in vertical direction, because of single sensor is using for measurements along of whole profile for each sounding (Bergman, 1978, Larsen at al., 1978, Alduchov, 1985). So, usually reported "standard observational errors" make an actual sense mostly for horizontal/time direction, not for vertical direction.

From the previous considerations the following deductions follows:

1) For detailed profiles (like GPS soundings) the observed upper-air parameters should be reported with accuracy at least 100 times better that in current practice (up to 0.001 °C for temperature, 0.001% for relative humidity and so on). Even it does not add the real accuracy (in the sense of horizontal/time observational errors) for the reported absolute values, but it will

allow getting much precise gradient profiles (because of high correlated observational errors). We understand that it is most unreal way to solve the problem, because of huge international regularizations of upper-air observations.

2) The smoothing methods should be used by researchers for estimations of any derivatives along of "actually observed" new detailed profiles of upper-air parameters.

More specific recommendations for CE-method for cloud detection on the base of radiosonde observations:

For detecting cloudiness boundaries by the CE-method in atmospheric layer 0-10 km with regular/interpolation cubic spline approximation for temperature and humidity profiles better to use the resolution of 300 -600 meters.

For detecting cloudiness boundaries by the CE-method in atmospheric layer near 0-1.5 km there is possibility to use more detailed profiles (with resolution near some tens of meters) by using smoothing spline approximation for temperature and humidity profiles [see, for example, Bartels et al.,1987].

Results can be used for modeling of atmospheric circulation and cloud modeling.

Acknowledgments. Drs. O. Alduchov and I. Chernykh are partly supported by Russian Basic Research Foundation (RBRF), projects 01-05-65285 and 01-05-64748.

References:

Alduchov O.A.1985: About structure of geopotential height and temperature observation errors. *RIHMI-WDC Proceeding*, Issue 131, 29-39 pp. (in Russian).

Bartels, R.H., J.C. Beatty, and B.A.Barsky, 1987:An Introduction to Splines for use in Computer Graphics and Geometric Modeling. *Morgan Kaufman Publishers*, 476 pp.

Bergman K.H.,1978: Role of observational errors in optimum interpolation analysis. – *BAMS,* Vol. 59, No. 12, p. 1603-1611.

Chernykh I.V. and R.E. Eskridge, 1996: Determination of cloud amount and level from radiosonde soundings. *J. Appl. Meteorology , **35,*** 1362-1369pp.

Chernykh I.V., O.A. Alduchov, R. E. Eskridge, 2001: Trends in low and high cloud boundaries and Errors in height determination of cloud boundaries. *BAMS,* **82,** 1941–1947.

Chernykh, I.V., and O.A. Alduchov, 2000: Comparison of cloud layers detecting by different methods. *The Fifth International Cloud Modelling Workshop, Working Group on Polar Clouds,* 7-11 August, Colorado. 22 p., http://paos.colorado.edu/~curryja/wg5/ca_comprfa.pdf

Hawson C. L., 1970: Performance requirements of aerological instruments. – WMO, Technical Note No. 112, (WMO – No. 267, TP.151), pp. 1-53.

Hooper A. H., 1975: Studies on radiosonde performance. – WMO, Technical Note No. 140. (WMO-No.394). Switzerland, Geneva. p. 1-110.

Larsen G,. Little G., Lorens a., Rutherford I., 1978: Analysis error calculations for FGGE. – *GARP Report*, No. 16, p. 55-117.

Naud C.M., Muller J.P. , E.E. Clothiaux, 2003: Comparison between active sensor and radiosonde cloud boundaries aver the ARM Southern Great Plains site. *J. Geophysical research*, Vol. 108, NO. D4, P. 3-1 – 3-12.

On Impact of Radiosondes' Shift into Objective Analysis[1]

Vladimir V.Bayev, Vladimir A.Gordin, *Hydrometeorological Center of Russia, Moscow, Russia*

The trajectories of a radiosonde ascend can be described by the following system:

$$\begin{cases} \dfrac{dx}{dt}(t) = U(x(t), y(t), \xi(t), t) \cdot b_x(y(t)), & x(0) = x_0 \\ \dfrac{dy}{dt}(t) = V(x(t), y(t), \xi(t), t) \cdot b_y, & y(0) = y_0 \\ \dfrac{d\xi}{dt}(t) = -\dfrac{\mu g \cdot (az_0 + b) \cdot e^{-a(t-t_0)}}{R \cdot T(x(t), y(t), \xi(t), t)}, & \xi(0) = \ln(p_0) \end{cases},$$

where x, y are latitude and longitude in minutes, $\xi = \log(p)$, p is pressure in hPa, t is time in minutes, U, V – fields of zonal and meridian wind's components in m/sec,

$b_y = \dfrac{60}{R_E \cdot \pi / 10800}$, $b_x(y) = b_y / \cos(y \cdot \pi / 10800)$ are corresponded coefficients of conversion for units of measurements of horizontal velocity (R_E is Earth's radius),

μ is molar mass of air,

g – acceleration of free falling,

R is the universal gas constant,

T is a temperature in Kelvin,

$\left.\begin{array}{l} a = 0.0058 \ \text{min}^{-1} \\ b = 274 \ \text{m/min} \end{array}\right\}$ – empirical constants for sonde's lifting: $\dfrac{dz}{dt} = az + b$, $z(t)$ is the sonde's height,

x_0, y_0, z_0, p_0 are latitude and longitude of a station, it's height over sea level and pressure in the sonde's launch moment t_0.

Table 1.

i	p_i ,gPa	$\langle t_i \rangle$,min	$\langle t_i \rangle_2$,min	$\langle \Delta X_i \rangle$,km	$\langle \Delta Y_i \rangle$,km	$\langle d_i \rangle_2$,km	$d_i^{\max}$,km	q_i
1	1000	-38.10	42.09	-0.02	-0.01	0.13	0.54	8050
2	925	-37.71	41.74	-0.03	-0.04	0.84	3.12	13392
3	850	-35.75	40.02	0.06	-0.07	1.88	7.46	14758
4	700	-30.68	35.58	1.01	-0.11	4.65	20.03	15326
5	500	-22.11	28.50	4.85	-0.32	11.10	44.51	15470
6	400	-16.93	24.69	8.69	-0.50	16.94	62.83	15471
7	300	-10.79	20.97	14.85	-0.66	26.06	87.92	15471
8	250	-7.17	19.36	19.33	-0.70	32.51	103.36	15471
9	200	-2.93	18.22	25.11	-0.74	40.49	121.61	15471
10	150	2.29	18.13	32.27	-0.78	49.92	147.50	15471
11	100	9.27	20.21	40.29	-0.87	60.10	174.34	15471
12	70	15.13	23.47	45.13	-1.01	66.09	190.69	15471
13	50	20.49	27.24	48.15	-1.15	69.73	200.51	15471
14	30	28.41	33.61	51.26	-1.40	73.43	208.71	15471
15	20	34.56	38.96	53.74	-1.60	76.41	213.57	15471
16	10	44.73	48.22	59.32	-1.84	82.81	237.69	15471

By the way we can take into account the exact place and moment of any concrete measurement. The statistics of the deviations see in Table 1. Here d_i is the distance in kilometers, q_i is the number of measurements in the ensemble, $\langle s \rangle$ is the average value of s, and $\langle s \rangle_2 = \sqrt{\langle s^2 \rangle}$.

[1] *The work was partly supported by the grant 01-05-64748a;* vagordin@vagordin.mccme.ru

We can see the shift of the measurements is significant and really can make worse the objective analysis results, especially on higher levels.

Can we reduce the errors if localize the measurement's point more exactly. To answer on the question we compare a meteorological value A with 1) first guess of A for horizontal coordinates of the corresponding station; 2) first guess of A for horizontal coordinates of the corresponding sonde. We denote these values $\Delta A^{\text{current}}$ and ΔA^{lifted}.

We use the following experiment to understand the maximal impact of exact sonde's localization. We compute first guess in the true time-space point of the concrete observation and compare with the result of this observation. These results are our goal for future investigation of the following Lagrangian model.

If we assume some meteorological value A is conserved in any particle, we should integrate the ordinary differential system

$$\frac{dA}{dt} = 0\,, \quad \text{where } \frac{d}{dt} = \frac{\partial}{\partial t} + U\frac{\partial}{\partial x} + V\frac{\partial}{\partial y} + W\frac{\partial}{\partial z}\,, \tag{1}$$

along the particle trajectory. We start in the true observation moment and finish in the basic moment $t = 0$ in a "traced" point. We obtain the initial data for A by the way. The coefficients of the system $U,V,W,$ can be obtained from a forecast model.

If the value A is not conserved, e.g. it is a component of horizontal wind, then we should use in the right hand-side some fields from the forecast, too:

$$-\frac{du}{dt} = \frac{\partial \Phi}{\partial x} - lv \quad , \quad -\frac{dv}{dt} = \frac{\partial \Phi}{\partial y} + lu\,. \tag{2}$$

Here it is geopotential $\Phi = \Phi(x, y, p, t)$. The approach can be useful for assimilation of any asynchronic meteorological data, e.g., from satellites and aircrafts.

In the Table 2 we demonstrate some improvement of concordance[2] with 12-h forecast of temperature (similar results for wind's components were obtained):

Table 2

i	p_i ,gPa	$\langle \Delta T_i^{\text{current}} \rangle_2$, K	$\langle \Delta T_i^{\text{lifted}} \rangle_2$, K	$\langle \Delta T_i^{\text{lifted0}} \rangle_2$, K	$\langle \Delta T_i^{\text{traced}} \rangle_2$, K	q_i
3	850	1.516	1.526	1.516	1.528	10238
4	700	1.123	1.121	1.121	1.124	10701
5	500	1.046	1.037	1.042	1.044	10780
6	400	1.033	1.028	1.030	1.034	10700
7	300	1.239	1.240	1.241	1.250	10532
8	250	1.349	1.341	1.341	1.339	10354
9	200	1.433	1.410	1.412	1.413	10152
10	150	1.365	1.347	1.349	1.352	9825
11	100	1.523	1.516	1.520	1.521	9543
13	50	1.659	1.640	1.642	1.652	7111

Now only 65% of TEMP messages include information on exact start moment (with minutes). We appeal meteorologists to do it.

V.A.Gordin. *Meteorological Data Assimilation as a Subject of Applied Mathematics.* Proc. Hydrometeorological Center of Russia 334, pp.69-78, 1999 (Russian).

V.A.Gordin. *Mathematical Problems and Methods in Hydrodynamic Weather Forecasting.* Gordon & Breach, 2000.

Triphonov G.A. "Approximation of a dependence of radiosonde radiation error from the Sun elevation and height", Proc. Centr. Aerol. Observ., Russia, 1983, N 151, pp.8-13.

[2] *Model (1) with the simple transport of A should be exchanged on model (2).*

Importance of vertical water vapor analysis
- A problem in assimilating TPW with 4DVar -

Teruyuki KATO[1], Yoshiaki SATO[2] and X-BAIU-01 observation group
[1]*Meteorological Research Institute / Japan Meteorological Agency, Tsukuba*
[2]*Meteorological Satellite Center / Japan Meteorological Agency, Kiyose*

1. Introduction

During the "Observation of Baiu front over East China Sea and Kyushu in 2001" (X-BAIU-01), the nonhydrostatic model (NHM, Saito et al, 2001) with a horizontal grid size of 5 km (5km-NHM) was operated twice a day to support the observations. 5km-NHM usually predicted rainfall successfully, while failing to do in a few cases. In the morning on 23 June, a band-shaped Mesoscale convective system (MCS) with strong precipitation intensity was observed over southern Kyushu (Fig. 1a), while 5km-NHM hardly predicted rainfall there (Fig. 1b). This MCS suddenly formed at 03 JST (= UTC + 9 hours) to the southwest of Kyushu Island, and rapidly developed. After 08 JST, the MCS stagnated over southern Kyushu until noon.

The purpose of the present study is to improve the prediction of heavy rainfall. The improvement of prediction is investigated when the initial fields are modified using the special observation data. Also the prediction is compared with the results in case of the Tropical Rainfall Measuring Mission Microwave Imager (TMI) data being assimilated to the mesoscale analysis of the JMA.

2. Numerical models

The NHM used in the present study is the full compressible version, in which the density is calculated directly from the state equation without any approximation. The sound waves are treated implicitly both in horizontal and vertical directions. The full scope of microphysics is used to explicitly predict the mixing ratios of cloud water, rainwater, cloud ice, snow, and graupel. For other specifications, see Table 1 in Kato and Goda (2001). The initial and boundary conditions are produced by interpolating the forecasts of Regional Spectral Model (RSM) with a 20-km resolution. The 6-hour forecast of RSM (starting at 00 JST and 12 JST, 22 June 2001) is used as the initial conditions.

3. Improvement of prediction

By comparing the observations with the simulations, the failure of heavy rainfall prediction could be resulted from the lower atmosphere being drier than it is in reality. Therefore, the initial lower atmosphere

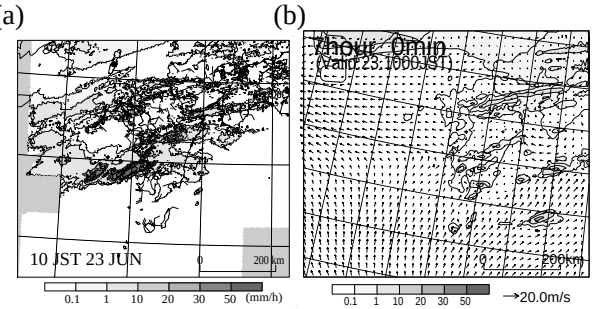

Fig.1 (a) Hourly accumulated rainfall at 10 JST on 23. (b) Same as (a), but for simulation by 5km-NHM.

of 5km-NHM over ocean southwest of Kyushu Island has to be humidified to reproduce the heavy rainfall. In the present study, two methods are used. One is called MOD that the relative humidity *rh* below a height of 1.5 km is increased to over 95 % for the TPW to be close to the TMI-derived TPW. The four-dimensional variational data assimilation technique (4DV) was used for another method. The initial field of 5km-NHM was produced by interpolating the mesoscale analysis with 4DV. In the present study, the TMI-derived TPW data was added to the mesoscale analysis (Sato et al, 2002).

Figure 2 shows the vertical cross section of *rh* in a south-north direction in the initial of 5km-NHM. The lower atmosphere in the control simulation (Fig. 2a) was considerably dry to the south of the area where the band-shaped MCS formed. This dry air made a small value of TPW in the control simulation. In the sensitive experiment with MOD (Fig. 2b), the lower atmosphere below a height of 1.5 km was nearly saturated, and a humid air was supplied into the area where the band-shaped MCS formed.

Figure 3 show the rainfall distributions simulated with MOD and 4DV. For MOD (Fig. 3a), the band-shaped rainfall with the precipitation intensity over 50 mm h^{-1} was reproduced successfully. But, it was simulated southward by 50 km in comparison with the observation (Fig. 1a).

For 4DV (Fig. 3b), rainfall areas were simulated over southern Kyushu. The location of the simulated band-shaped MCS was closer to the observation than that for (Fig. 3a). However, the structure of the simulated band-shaped MCS was not reproduced well, and the simulated precipitation intensity was not strong enough to forecast a heavy rainfall. Noted that the atmosphere below a height of 3.5 km was nearly

*Corresponding author address: Teruyuki Kato, Meteorological Research Institute, 1-1 Nagamine, Tsukuba, Ibaraki 305-0052 Japan: e-mail: tkato@mri-jma.go.jp

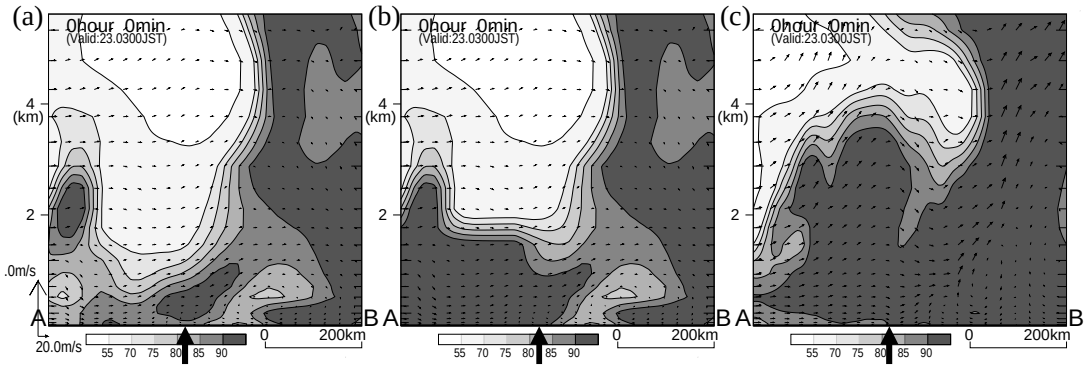

Fig. 2 The vertical cross section of *rh* in a south-north direction in (a) the control simulation, and sensitive experiments with (b) MOD and (c) 4DV. Bold arrows denote the location of the band-shaped MCS forming.

saturated to the upstream of the area where the band-shaped MCS formed at 04 JST (Fig. 2c). Such a weak convectively unstable layer cannot induce a heavy rainfall. The 4DV cannot well retrieve the vertical profile of water vapor only using the TPW data. This result indicates that the vertical water vapor analysis is significant to simulate a heavy rainfall.

4. Conclusion

Good accuracy in the analysis of a vertical water vapor profile is necessary for the NHM to forecast heavy rainfalls during the Baiu season. Especially, the accuracy over the East China Sea, i.e., the upstream of the Baiu frontal zone, is significant. However, few upper-air soundings are operated there. Therefore, the 4DV analysis using the TPW retrieved from satellite data such as TMI data is expected to improve the water vapor field. However, it is difficult to reproduce the vertical profile of water vapor from TPW data. This is.because, when the TPW is assimilated by 4DV, the water vapor at all vertical grids is increased or decreased at the same rate in proportion to the amount of TPW, i.e., it is impossible to humidify only the lower atmosphere (Fig. 4b). Although the lower atmosphere can be mainly modified by setting a weight function in 4DV to reproduce the present heavy rainfall (Fig. 4a), this modification cannot be applied to whole areas and all seasons

Spatially and temporally dense upper-air soundings are necessary in order to use TPW data effectively. This is because the estimation of a water vapor field among upper-air sounding points is difficult due to its being a passive tracer, while dynamical fields such as temperature and wind can be reasonably interpolated by 4DV. These dense soundings may be replaced in the near future by remote-sensing observations from the ground and satellites. Furthermore, spatial observations of low-level water vapor, such as those made by aerosondes, are significant because the water vapor over the sea south of the Baiu frontal zone concentrates in the lower atmosphere and few upper-air soundings are conducted there.

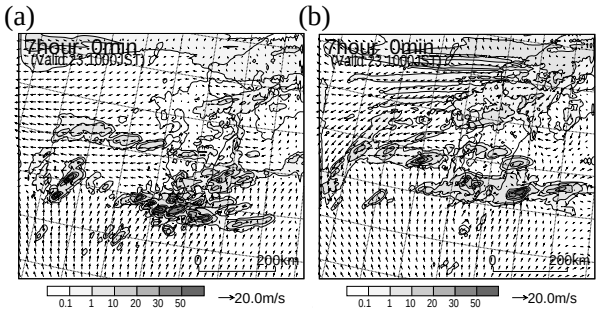

Fig. 3 Same as Fig. 1, but for sensitive experiments with (a) MOD, and (b) 4DV.

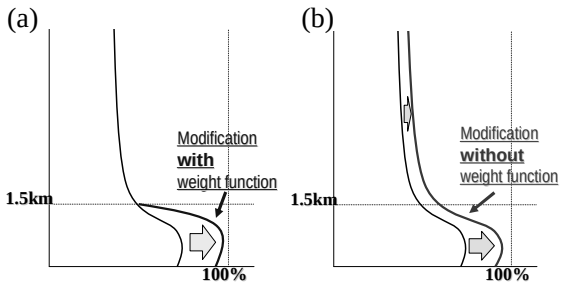

Fig. 4 Modification of water vapor profile by assimilating TPW using 4DV (a) with and (b) without weight function in areas without rain.

Refferences

Kato, T. and H. Goda, 2001: Formation and maintenance processes of a stationary band-shaped heavy rainfall observedin Niigata on 4 August 1998. *J. Meteor. Soc. Japan*,**79**, 899-924.

Saito, K., T. Kato, H. Eito and C. Muroi, 2001: Documentation of the Meteorological Research Institute / Numerical Prediction Division Unified Nonhydrostatic Model. *Tech. Rep.of MRI*, **42**, p133.

Sato, Y., K. Koizumi, T. Tauchi, and M. Kachi, 2002: The assimilation experiment of TMI precipitation/total precipitable water using the four-dimensional variational method, *Proc of 2002 autumn meeting of Meteo. Soc. of Japan*, **82**, A307 (in Japanese).

Assimilating long-duration balloon data using a Partial OSSE

Michael Keil
Met Office, London Road, Bracknell, UK, RG12 2SZ
michael.keil@metoffice.com

Stratospheric long-duration balloons offer a potentially abundant supply of in-situ data. Various projects, such as the Global Air-ocean IN-situ System (GAINS) and the Ultra-Long Duration Balloon (ULDB), are currently planning to regularly fly balloons in the stratosphere, with the ultimate aim of constructing a global network of balloons. Balloon platforms can host an array of instruments enabling a wide range of atmospheric constituents and behaviour to be monitored. It is important that the impact on NWP from assimilating data from balloon constellations is understood before they become part of the global observation network.

To estimate the performance of a constellation of long-duration stratospheric balloon data, it is necessary to simulate balloon observations. A hybrid experiment, which is a cross between an Observation Systems Experiment (OSE) and an Observation System Simulation Experiment (OSSE), called a Partial Observation System Simulation Experiment (POSSE) was developed. POSSEs allow a mix of real and simulated data to be assimilated. Data from balloon constellations were simulated from a nature analysis, in this case provided by ECMWF. The simulated data was subsequently assimilated into the Met Office Stratospheric 3D-Var system along with a degraded set of real observations. The volume of ATOVS data was deliberately reduced in the real observation set, thus ensuring that atmospheric information was contained within the simulated data. A similar procedure to the POSSE, called an Observation System Replacement Experiment (OSRE), has been performed at Deutscher Wetterdienst to test the effect of assimilating lidar wind data (Wergen, 2000). Horizontal wind data for five different configurations of simulated balloon constellations were assimilated for January 2001. The networks consisted of 410, 205, 103 and 52 drifting balloons, plus a static constellation containing 410 balloons, all flying at an altitude of 30hPa.

Analyses and forecasts from the POSSE and control runs were verified against the nature run. Overall, the POSSE produced a measurable improvement in the rms horizontal windspeeds in all cases at the balloon flight level, 30hPa. This can be seen in figure 1, where increasing the constellation density increases the accuracy of the analysis. There is no clear evidence in this experiment to suggest whether it is more beneficial to have drifting or static balloon constellations. Figure 2 shows the fractional (normalised) rms benefit at all vertical levels. The global average, in the left hand plot of figure 2, is dominated by the signal from the tropics. The largest rms horizontal windspeed improvement was found in the in tropics, although the benefit had limited vertical extent. In the extra-tropics, right hand plot in figure 2, the vertical extent of the windspeed benefit was much greater, with the whole depth of the stratosphere affected. The results from the POSSE are very encouraging and indicate that adding a permanent constellation of stratospheric balloons to the global observing system would be beneficial to the NWP community.

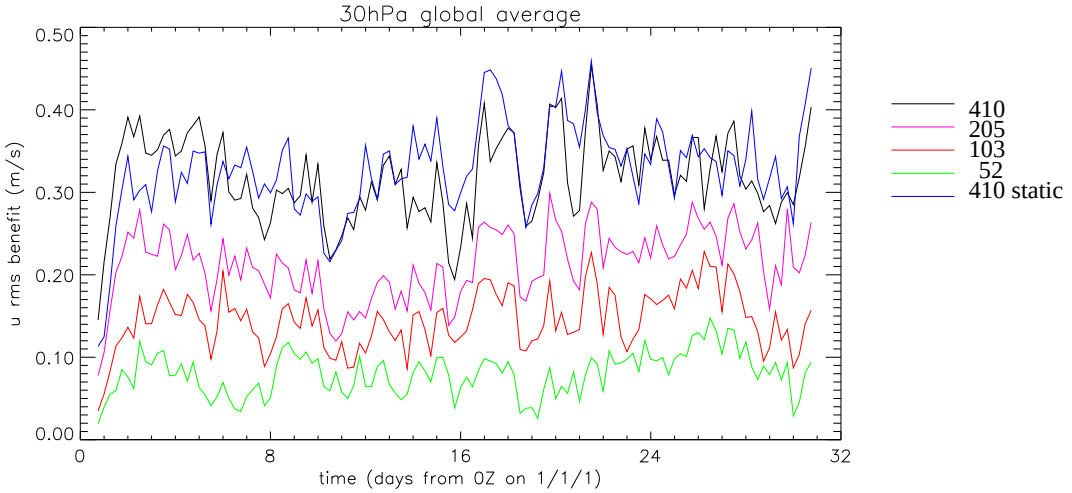

Figure 1: Timeseries of the rms benefit (rms control - rms POSSE, relative to nature) in the zonal wind field at 30hPa. Positive values indicate the POSSE is closer to the nature run.

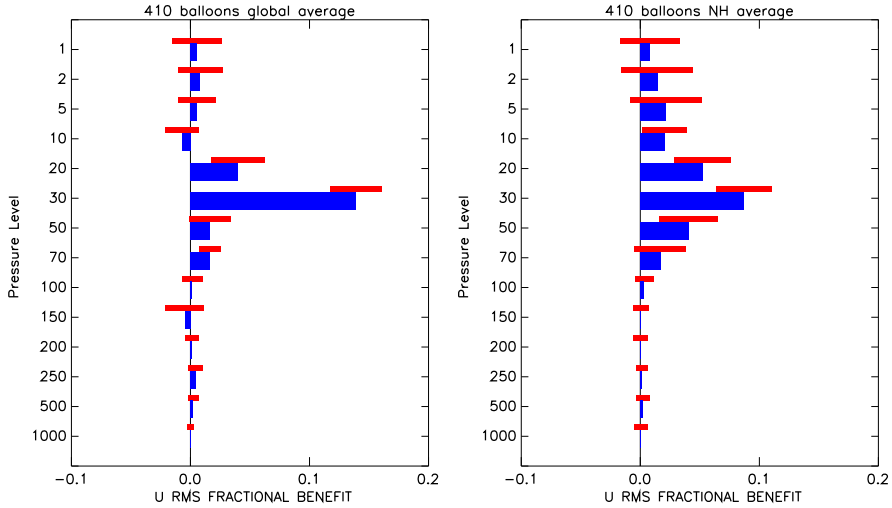

Figure 2: Histograms of the fractional zonal wind rms benefit for the 410 balloon constellation (thick rectangles). The thin rectangles represents the $\pm 1\sigma$ error bounds. The left hand plot is a global average and the right hand plot is a NH average (30°N-90°N).

Wergen, W., Impact studies for a proposed European space-borne wind lidar instrument, *Proceedings of the second CGM/WMO workshop on the impact of various observing systems on numerical weather prediction, Toulouse, France, 6 -8 March 2000, World Weather Watch Technical Report No. 19, WMO/TD No. 1034*, 199 - 202, 2000.

A suboptimal Kalman filter algorithm with the simplified models for calculation of the forecast error covariances

Dr. Ekaterina G. Klimova
Institute of Computational Technologies,
Siberian Branch, Russian Academy of Sciences,
Ac. Lavrentjev Avenue, 6
Novosibirsk 630090 Russia
klimova@ict.nsc.ru

The most fundamental difficulties of the implementation of the Kalman filter theory to the meteorological data assimilation are that it is too computationally expensive and requires too much information. One of the ways to solve this problem is to apply the simplified models in a Kalman filter for calculation of the forecast error covariances.

We shall proceed from the concept of decomposition of the dynamic operator of prognostic model. Let us present a system of prognostic equations as

$$\frac{d\phi}{dt} = A_1\phi + A_2\phi,$$

where ϕ - vector of forecast fields. The operator A_1 describes an advection of mass and temperature along trajectories of motion, operator A_2 - process of adaptation of a wind and geopotential fields. Let us consider initial model on a small time interval (t_k, t_{k+1}) and use the velocity components in the advection operator A_1 at time t_k. Then the model will be linear on this time interval. So, we consider the following models for calculation of matrices of the forecast errors covariances.

Suppose, that the true atmospheric flow is described by the baroclinic adiabatic model of atmosphere for region based on the primitive equations (we shall name it model-0).

Model-1 is proposed in [1] and is obtained under following assumptions:

- an estimation of the atmospheric fields using the Kalman filter is carried out for the vertical normal modes of the forecast model;
- the calculation of the forecast error covariances is based on the assumption that the errors of vertical normal modes do not correlate; moreover, the forecast error covariances are calculated only for the geopotential field and the wind forecast error covariances are derived from them under the geostrophic assumption;
- the forecast model of our system is based on the method of splitting into the physical processes and we use only the advection step for the calculation of the forecast error covariances;
- the background fields of velocity components in the advection operator do not depend on vertical coordinate p (i.e., the background flow is close to barotropic).

Thus the model is described by the equation of advection for the coefficient of the height field h_n of n-th vertical normal mode.

In [4] is shown, that such simplified model is justified, in particular, in a case, when the forecast error covariances are homogeneous and isotropic**.** An analytical equation for a local covariance of forecast errors between two specified points is obtained in [4]. From this equation

follows, that dynamics of covariances of errors of the forecast, in case they are homogeneous and isotropic, on a small time interval is described by model of advection of substation on trajectories of particles.

However, the atmospheric motion of large scales is not homogeneous and isotropic. At the same time it is known, that the large-scale atmospheric flows are well described with the help of quasigeostrophic approximation. Thus, we shall consider the following «hybrid» model: for the calculation of the forecast error covariances of first, large-scale vertical normal modes, the linearized quasigeostrophic equation is used and for others we use the model-1. With the described above simplified model the identical twins data assimilation experiments were carried out. The matrix of model errors was considered zero. In figure the time evolution of rms forecast error for the height of 500 mb is presented. In this figure s1 is the error of data assimilation based on the suboptimal Kalman filter algorithm with "hybrid" simplified model, s2 – the forecast error of traditional data assimilation algorithm with the use of optimal interpolation for the data analyses, s0 is the error of forecast without data assimilation. The main results are published in [1-5].

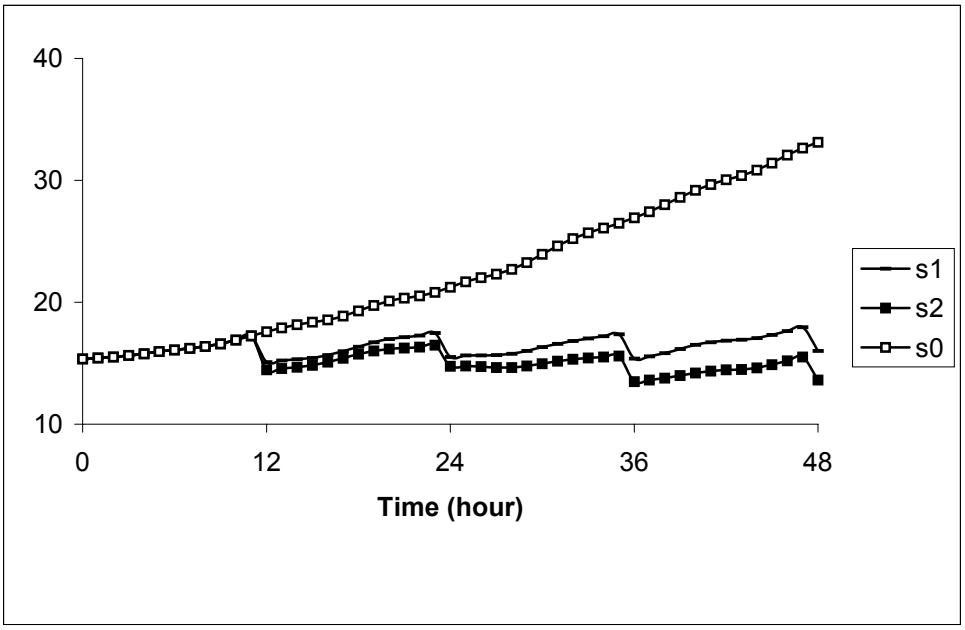

References

1. E.G.Klimova. Algorithm of the data assimilation of meteorological observations based on the extended suboptimal Kalman filter. - Russian Meteorology and Hydrology, 1997, N 11.
2. E.G.Klimova. Asimptotic behavior of the data assimilation scheme, based on algorithm of a Kalman filter. - Russian Meteorology and Hydrology, 1999, N 8.
3. E.G.Klimova. Simplified models for calculation of covariance matrices in the Kalman filter algorithm. - Meteorologiya i Hydrologiya, 2000, N 6. (Translated on English: Russian Meteorology and Hydrology).
4. E.G.Klimova. A model to calculate the covariances of homogeneous isotropic stochastic fields of forecast errors. - Meteorologiya i Hydrologiya, 2001, N 10.
5. E.G.Klimova. Model for calculation the forecast error covariances in the Kalman filter algorithm based on the full quations. - Meteorologiya i Hydrologiya, 2001, N 11.

Case Study on the Impact of Radar-derived TREC Winds on Model Forecast of Heavy Rain Associated with Landfalling Tropical Cyclone

C.C. Lam
Hong Kong Observatory, Hong Kong, China
cclam@hko.gov.hk

The initialization of numerical simulations using radar-derived winds has been studied for around a decade (Crook and Tuttle, 1994). In recent years, applications of radar data in operational mesoscale models become increasingly popular. Many techniques exist for retrieving horizontal winds from radar data, including dual-Doppler, TREC (Tracking Radar Echoes by Correlation), reflectivity conservation methods (Qiu and Xu, 1992; Laroche and Zawadsky, 1993; Shapiro, 1993) and the adjoint method applied to the radial momentum equation (Xu *et al*., 1993).

This study assessed the potential of the application of TREC winds in initializing tropical cyclones, using the case of tropical cyclone Kammuri (0212) in 2002. Numerical experiments on the assimilation of TREC winds were performed at the Hong Kong Observatory (HKO) using the hydrostatic Operational Regional Spectral Model (ORSM) and the non-hydrostatic Advanced Regional Prediction System (ARPS). The TREC method was based on the assumption that reflectivity features are transported by the local flow. It was originally adapted for use in the HKO for nowcasting purpose (Li *et al*., 2000).

The ORSM was configured to run at a 20-km inner domain one-way nested inside a 60-km domain with 36 vertical levels. The ARPS was run at a 6-km inner domain one-way nested inside a 30-km outer domain with 40 levels. The boundary conditions of both outer models were provided by the Global Spectral Model (GSM) of Japan Meteorological Agency (JMA). The ORSM employs 3-dimensinal multivariate optimal interpolation. The ARPS Data Assimilation System (ADAS) adopts the Bratseth successive correction scheme. In the ADAS, radar velocity and reflectivity data were assimilated. The Doppler radar velocity data were utilized to calculate increments to the horizontal winds by estimating the Cartesian component increment from the radial winds.

The impact of TREC winds on model rainfall forecasts was evaluated with and without the presence of tropical cyclone bogus data. TREC winds at 1 km and 3 km levels were assimilated in the models. Figure 1(a) and (b) shows the radar reflectivity data and the radar-derived TREC winds at 3-km level valid at 18 UTC 4 August 2002 respectively. The circulation of Kammuri was well depicted by the TREC winds.

With the assimilation of TREC winds, the ARPS predicted generally higher rainfall intensities in the first few hours (Fig.2(a) vs. Fig.2(b)). The impact was still observable in later forecast hours (figures not shown). For the ORSM, the impact of TREC winds was less prominent that that of ARPS (Fig.3(a) vs. Fig3(b)). The ORSM was not very sensitive to the use of TREC wind data. Instead, the effect of TC bogus data was significant (figures not shown).

Indications are that additional radar derived wind data like TREC winds with finer vertical resolution may produce a more substantial impact on the rainfall forecasts of tropical cyclone upon landfall. Further experimentation with TREC winds with finer vertical resolution in addition to Doppler velocity data will be carried out. Effort will continue in the development of better methods to utilize radar in mesoscale models, particularly for the forecasting of winds and rain associated with landfalling tropical cyclones.

References

Crook, A., and J.D. Tuttle, 1994: Numerical simulations initialized with radar-derived winds. Part II: Forecasts of three gust-front cases. *Mon. Wea. Rev*., **122**, 1204-1217.

Laroche, S., and I. Zawadzki, 1993: Echo tracking by three variational analysis methods. *Proc. 26th Int. Conf. on Radar Meteorology*, Norman, OK, Amer. Meteor. Soc., 438-440.

Li, P.W., W.K. Wong, K.Y. Chan, and E.S.T. Lai, 2000: SWIRLS – An Evolving Nowcasting System. Technical Note, No. 100, Hong Kong Observatory.

Qiu, C.-J., and Q. Xu, 1992: A simple adjoint method of wind analysis for single-Doppler data. *J. Atmos. Oceanic Technol*., **9**, 588-598.

Shapiro, A., 1993: A single-Doppler velocity retrieval in the convective boundary layer. *Proc. 26th Int. Conf. on Radar Meteorology*, Norman, OK, Amer. Meteor. Soc., 441-443.

Xu, Q., C.-J. Qiu, J.-X. Yu, H.-D. Gu, and M. Wolfson, 1993: Adjoint-method retrievals of microburst winds from TDWR data. *Proc. 26th Int. Conf. on Radar Meteorology*, Norman, OK, Amer. Meteor. Soc., 433-434.

Acknowledgments

The ORSM was developed based on the RSM of Japan Meteorological Agency. The ARPS was originally developed by CAPS of the Univeristy of Oklahoma.

(a) (b)

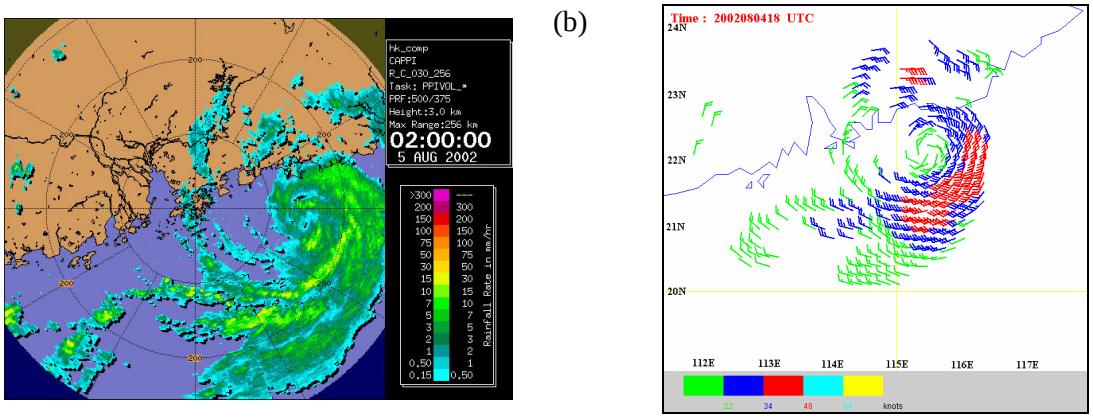

Fig.1 (a) Rainfall reflectivity and (b) radar-derived TREC winds at 3-km level valid at 18 UTC 4 August 2002.

(a) (b)

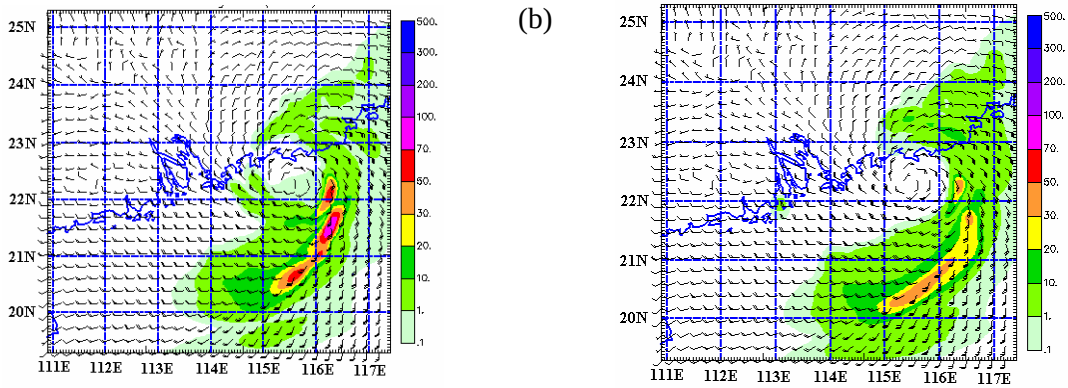

Fig.2 6-km ARPS T+3 h forecast for 3-hourly accumulated rainfall (mm) and surface winds (a) with TREC wind data and (b) without TREC wind data. The model valid time is 21 UTC 4 August 2002.

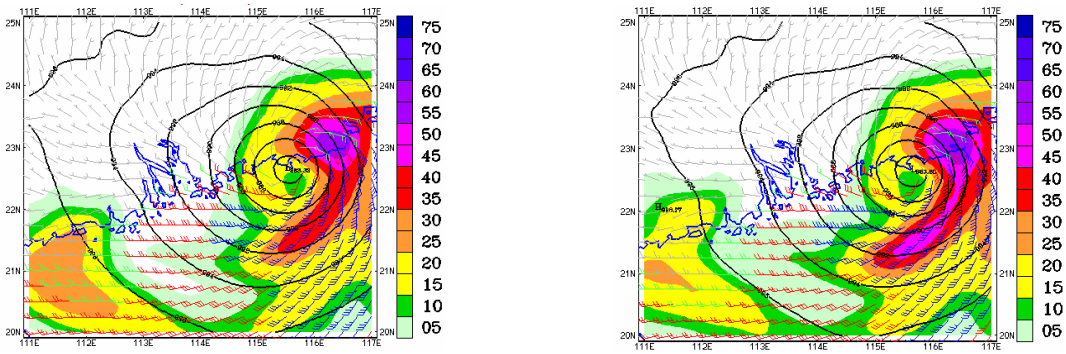

Fig.3 Same as Fig.2 except for 20-km ORSM.

ESTIMATION OF OBSERVATION VALUE USING THE NAVDAS ADJOINT SYSTEM

Rolf H. Langland
Naval Research Laboratory, Monterey, CA 93943
langland@nrlmry.navy.mil

A new adjoint-based "observation impact" procedure has been developed for assessing the value (in terms of forecast impact) of any or all observations used in a data assimilation / forecast system. The procedure can be applied as a diagnostic tool to monitor the assimilation and quality control of any observation type, and can also be used in the design of improved observing networks. It can be applied to any forecast and data assimilation system for which adjoints exists. Here we describe implementation using the Navy Operational Global Atmospheric Prediction System (NOGAPS) and the NRL Atmospheric Variational Data Assimilation Procedure (NAVDAS).

The calculation of observation impact uses the adjoints of both NOGAPS and NAVDAS. We seek the gradient ($\partial J/\partial \mathbf{y}$) of a forecast error costfunction (J) with respect to the vector of observations ($\mathbf{y}$).

We first define a forecast error norm:

$$\mathbf{e}_\mathrm{f} = \left\langle \left(\mathbf{x}_\mathrm{f} - \mathbf{x}_\mathrm{a}\right), \mathbf{C}\left(\mathbf{x}_\mathrm{f} - \mathbf{x}_\mathrm{a}\right)\right\rangle \quad , \quad (1)$$

where $\mathbf{x}$ is the vector of model predictive variables, vorticity, divergence, potential temperature, and surface pressure (humidity is predicted by the model but not used in the error norm calculation). The subscripts, f and a, refer to "forecast" and verifying "analysis", respectively, of the NOGAPS forecast and assimilation. In (1) $\mathbf{C}$ is a matrix of energy weighting coefficients that represents dry total energy. An energy metric is used because it is an appropriate choice for applications to predictability in the absence of an acceptable estimate of the actual analysis error covariance metric. The brackets $\langle\ ,\ \rangle$ represent a Euclidean inner product $\langle \mathbf{x}, \mathbf{y} \rangle = \Sigma\, \mathbf{x}_i\, \mathbf{y}_i$. The error norm in (1) has units of J kg^{-1}, and is summed between the lowest near-surface model level and a level near 150 hPa. The forecast verification area (FVA) in which the error is calculated can be any region, including the complete global domain. The costfunction for the adjoint gradient calculations is defined as $J_f = \frac{1}{2}\mathbf{e}_\mathrm{f}$ and the starting condition for the adjoint integration, at forecast verification time is:

$$\partial J_\mathrm{f} \big/ \partial \mathbf{x}_\mathrm{f} = \mathbf{C}\left(\mathbf{x}_\mathrm{f} - \mathbf{x}_\mathrm{a}\right) \quad . \quad (2)$$

One integration of the forecast model (NOGAPS) adjoint provides a three-dimensional sensitivity vector for the initial conditions (t=0):

$$\partial J_\mathrm{f} \big/ \partial \mathbf{x}_0 = \mathbf{L}^\mathrm{T}\, \partial J_\mathrm{f} \big/ \partial \mathbf{x}_\mathrm{f} \quad , \qquad (3)$$

where $\mathbf{L}^\mathrm{T}$ is the operator representing the adjoint of the discretized NOGAPS model. This adjoint sensitivity is obtained in a tangent linear and perfect model framework, and is linearized with respect to a trajectory provided by the nonlinear global forecast model (including moist physics), that is updated every

second time step (2Δ t = 1800 s). The second step in the sensitivity calculations is to extend the initial condition sensitivity gradient into observation space using the adjoint of NAVDAS:

$$\partial J_f / \partial \mathbf{y} = \mathbf{K}^{\mathrm{T}} \, \partial J_f / \partial \mathbf{x}_0 \quad , \qquad (4)$$

where $\mathbf{K}^{\mathrm{T}}$ is the operator representing the adjoint of the Kalman gain matrix in the data assimilation procedure. The quantity $\partial J_f / \partial \mathbf{y}$ is the sensitivity of the forecast error costfunction with respect to the complete set of observations, **y**, in observation space. If we consider that the background ($\mathbf{x}_b$) is fixed, then $\partial J_f / \partial \mathbf{y}$ is also the sensitivity to the innovations (observation – background). It should be noted that it is necessary to interpolate the sensitivity gradient $\partial J_f / \partial \mathbf{x}_0$, which is obtained on the forecast model grid in (3), onto the analysis grid before it can be used in (4), and care must be taken in this step to consider special properties of the sensitivity gradient.

We can use observation sensitivity gradients provided by (4) to estimate the impact of observations on various measure of short-range forecast error. Once calculated, the observation impact can then be correlated with other quantities such as background or observation error to identify potential problems in quality control or statistics used in the assimilation, or to investigate other research issues. For example, Fig. 1 depicts the correlation of observation impact with cloud cover, demonstrating that observations in cloudy regions have more impact on 72hr global forecast error. Fig. 2 depicts the sensitivity of 72hr global forecast error to ATOVS observation at one assimilation time. Accuracy of the observation sensitivity calculations is relatively good, even when applied to forecasts as long as 72h. Additional details about results and procedures used in observation impact calculations can be obtained from the author.

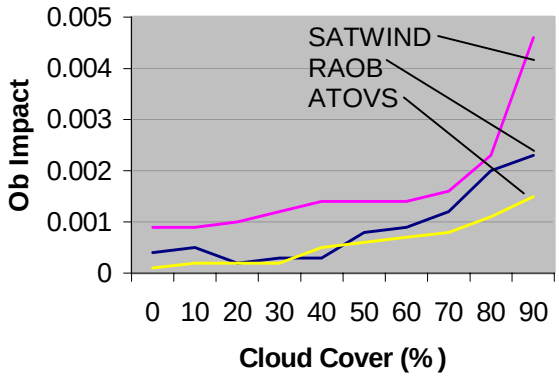

Fig. 1: Observation impact (average magnitude per observation type) on 72hr global forecast error (J kg^{-1}) as a function of model-diagnosed cloud-cover. Based on results from 29 June – 28 July 2002.

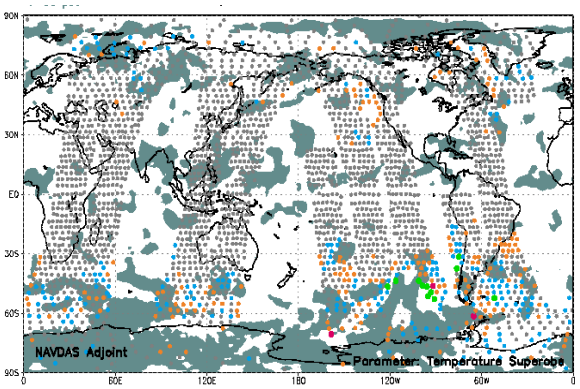

Fig. 2: Impact of ATOVS temperature profiles on 72 hr global forecast error for the assimilation at 00UTC 6 Sep 2002, with forecast verification at 00UTC 9 Sep 2002. Color dots indicate higher impact. Shading indicates diagnosed cloud cover > 60 percent. Each dot represents the combined impact of ~30 temperature observations in a profile through the entire depth of the troposphere.

The convergence of incremental 4D-Var using non-tangent linear models

A.S. Lawless and N.K. Nichols

Department of Mathematics, The University of Reading, UK.
email: A.S.Lawless@reading.ac.uk

The incremental formulation of 4D-Var allows the use of a linear model which is not exactly tangent to the discrete nonlinear model. One method of developing such a model is to discretize the continuous linear equations, forming a perturbation forecast model (PFM). Lawless *et al.* (2003) showed that a PFM can describe accurately the evolution of a perturbation in the discrete nonlinear model, provided that the perturbation is of a reasonable size, but for very small perturbations this is not the case. The present study considers the effects of using a PFM instead of a tangent linear model (TLM) within the inner loop of an incremental 4D-Var system.

The system used to test these effects is the one-dimensional shallow-water equations in the absence of rotation, which contains two variables, a wind field u and a mass field ϕ. The nonlinear model uses a semi-implicit semi-Lagrangian scheme, the TLM is derived directly from the discrete nonlinear model and the the PFM is derived by discretizing the continuous linearized equations of the system. The discretization is over 1000 grid points, with a distance $\Delta x = 0.01m$ between them. Further details of the model schemes can be found in Lawless *et al.* (2003).

We consider a situation in which a shock forms in the solution by the end of the assimilation window, so that we expect nonlinearities to arise and so differences between the two linear models to be highlighted. Identical twin experiments are performed using an incremental 4D-Var scheme, with both a TLM and a PFM. No background term is included in the cost function.

For the first experiment we run for a total of 12 outer loops and within each inner loop we converge until the norm of the gradient of the cost function is reduced by a factor of 10^4, with a restriction on the maximum number of inner iterations. Figure 1 shows the convergence of the cost function and its gradient for the two assimilations. We find that the convergence of the assimilation using the PFM follows very closely that using the TLM, despite the fact that the two models behave differently as the perturbation size is reduced. In Figure 2 we show the true solution for the wind field u at the end of the assimilation window and the analysis error from both assimilation runs. Even though the flow is highly nonlinear, both assimilations are able to analyse the true state to a high degree of accuracy. From the plot of analysis errors we see that both analyses are very close and the difference between them is no greater than would be expected from the convergence criterion used. The analyses for the ϕ field show similar errors to the u field analyses.

In order to test the assimilation as the perturbations become very small, we increase the convergence tolerance in each inner loop, requiring that the gradient norm be reduced by a factor of 10^8, again within a maximum number of inner iterations. Figure 3 shows a comparison of the convergence for the two different assimilations for this experiment. We see that the final value of the cost function is much reduced with respect to the first experiment. However, the two linear models continue to follow a very similar convergence pattern and again we find that the final analyses are very similar (not shown). Work is now in progress to develop a more complete theoretical explanation for these results.

References

Lawless, A.S., Nichols, N.K. and Ballard, S.P. (2003) A comparison of two methods for developing the linearization of a shallow-water model, *Q.J.R.M.S.*, **129**, 1237-1254.

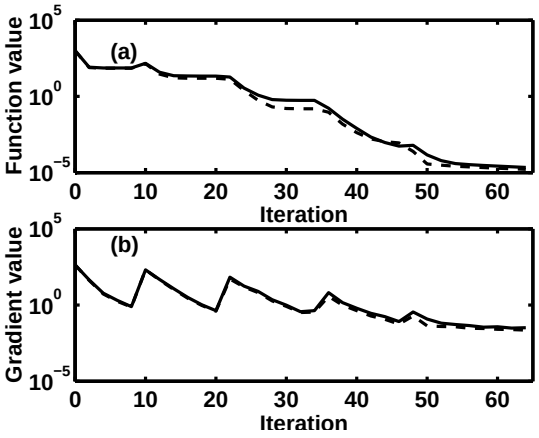

Figure 1: Convergence of (a) cost function and (b) gradient for assimilation using the tangent linear model (solid line) and the perturbation forecast model (dashed line).

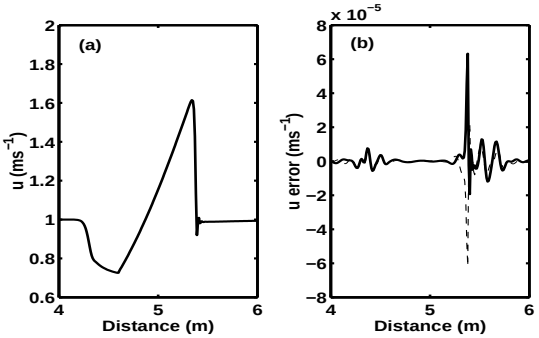

Figure 2: Analysis in u field at end of assimilation window. Plot (a) shows the true solution and plot (b) shows the analysis error for the TLM assimilation (solid line) and the PFM assimilation (dashed line).

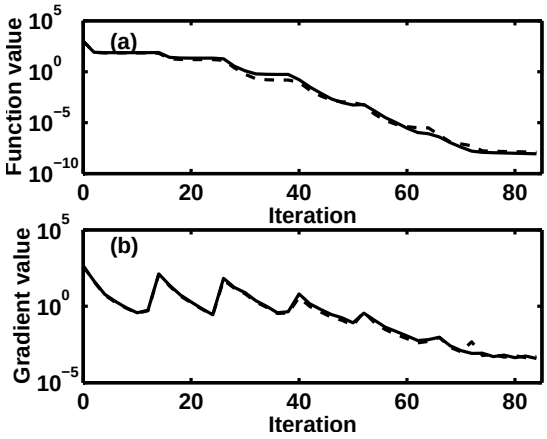

Figure 3: Convergence of (a) cost function and (b) gradient for assimilation using the tangent linear model (solid line) and the perturbation forecast model (dashed line).

Rain Quality Control for SeaWinds Near Real-time Data

S. Mark Leidner*, Ross N. Hoffman, and Mark C. Cerniglia
Atmospheric and Environmental Research Inc., Lexington, Massachusetts

1. Introduction

SeaWinds on QuikSCAT, launched in June 1999, provides a new source of surface wind information over the world's oceans. The primary mission of the SeaWinds instrument on the QuikSCAT satellite is to retrieve the surface vector wind over the global ocean (Shirtliffe 1999). This new window on global surface vector winds has been a great aid to real-time operational users, especially in remote areas of the world. As with in situ observations, the quality of remotely-sensed geophysical data is closely tied to the characteristics of the instrument. But remotely-sensed scatterometer winds also have a whole range of additional quality control concerns different from those of in situ observation systems. The retrieval of geophysical information from the raw satellite measurements introduces uncertainties but also produces diagnostics about the reliability of the retrieved quantities.

SeaWinds is an active, Ku-band microwave radar operating near $14\,Ghz$ and is sensitive to centimeter-scale or capillary waves on the ocean surface. These waves are usually in equilibrium with the wind. Each radar backscatter observation samples a patch of ocean about $25\times\ 35\ km$. The vector wind is retrieved by combining several backscatter observations made from multiple viewing geometries as the scatterometer passes overhead. The resolution of the retrieved winds is $\sim 25\ km$. Backscatter from capillary waves on the ocean surface, therefore, is the desired signal, since therein lies information about the vector wind. However, many other factors can influence backscatter observations and thereby effect the retrieved winds. Rain, for example, changes the ocean surface roughness, as well as attenuating and scattering the radar energy.

2. Rain Contamination

Many of the special characteristics of a scatterometer data are revealed by examining the likelihood function which is maximized during the wind retrieval. The closer the likelihood function is to zero, the more likely the wind solution. In Fig. 1, the upper panel shows a highlighted row of selected wind vectors (QuikSCAT rev 6659, 2207 UTC 28 September 2000) while the lower three panels show likelihood functions for selected cells. The underlying infrared satellite image shows Hurricane Isaac (2215 UTC 28 September 2000). Cells 41 and 36 are rain free according to the rain flags which accompany the data, but cells 40-37 (in blue) are affected by the heavy rain in the front.

The well-known ambiguity of wind direction in scatterometer data is apparent when the likelihood function is plotted with respect to the retrieved values of the u and v wind components. Likelihood functions for the the rain-free wind vector cells (41 and 35) show deep and distinct minima (two each). These minima represent likely wind solutions. The rain-affected wind vector cells (39, for example) however, have minima which are much further from zero, and are not nearly so well-defined. Also notice rain has nearly doubled the wind speed compared to neighboring rain-free cells. Rain has equalized backscatter for cell 39 from all view points and virtually no wind direction signal remains.

Rain flags were developed for SeaWinds after the launch of QuikSCAT. Original plans paired SeaWinds with a passive microwave sensor that would have provided a rain flag. Instead a variety of alternative rain flags have been proposed (Boukabara et al. 2002), and several of these have been combined into a multi-dimensional histogram (MUDH) rain indicator and rain flag (Huddleston and Stiles 2000).

SeaWinds and other scatterometer data in general have many potential uses, but it is important to understand their peculiar error characteristics for proper quality control and application.

References

Boukabara, S.-A., R. N. Hoffman, C. Grassotti, and S. M. Leidner, 2002: Physically-based modeling of QSCAT SeaWinds passive microwave measurements for rain detection. *J. Geophys. Res.*, **107**, 10.1029/2001JD001243.

Huddleston, J. N. and B. W. Stiles, 2000: A multidimensional histogram rain-flagging technique for SeaWinds on QuikSCAT. *Proc. Int. Geoscience and Remote Sensing Symp. (IGARSS)*, IEEE, New York, Honolulu, Hawaii, 1232–1234.

Shirtliffe, G. M., 1999: QuikSCAT science data product user's manual, overview and geophysical data products. Version 1.0, Jet Propulsion Laboratory, Pasadena, CA, [JPL D-18053].

* *Corresponding author address:* S. Mark Leidner, Atmospheric and Environmental Research, Inc., 131 Hartwell Avenue, Lexington, Massachusetts 02421; email leidner@aer.com

Fig. 1: *An example of rain-contaminated winds from SeaWinds. The upper panel shows the wind vector cell row of interest in bold wind barbs. Winds suspected of rain contamination are blue. The panels below show the QuikSCAT objective wind retrieval function for cells 41, 39 and 36. Notice that the wind speeds for cell 39 are very large compared to its neighbors, and the minima in the objective function are much larger than in adjacent, non-raining cells.*

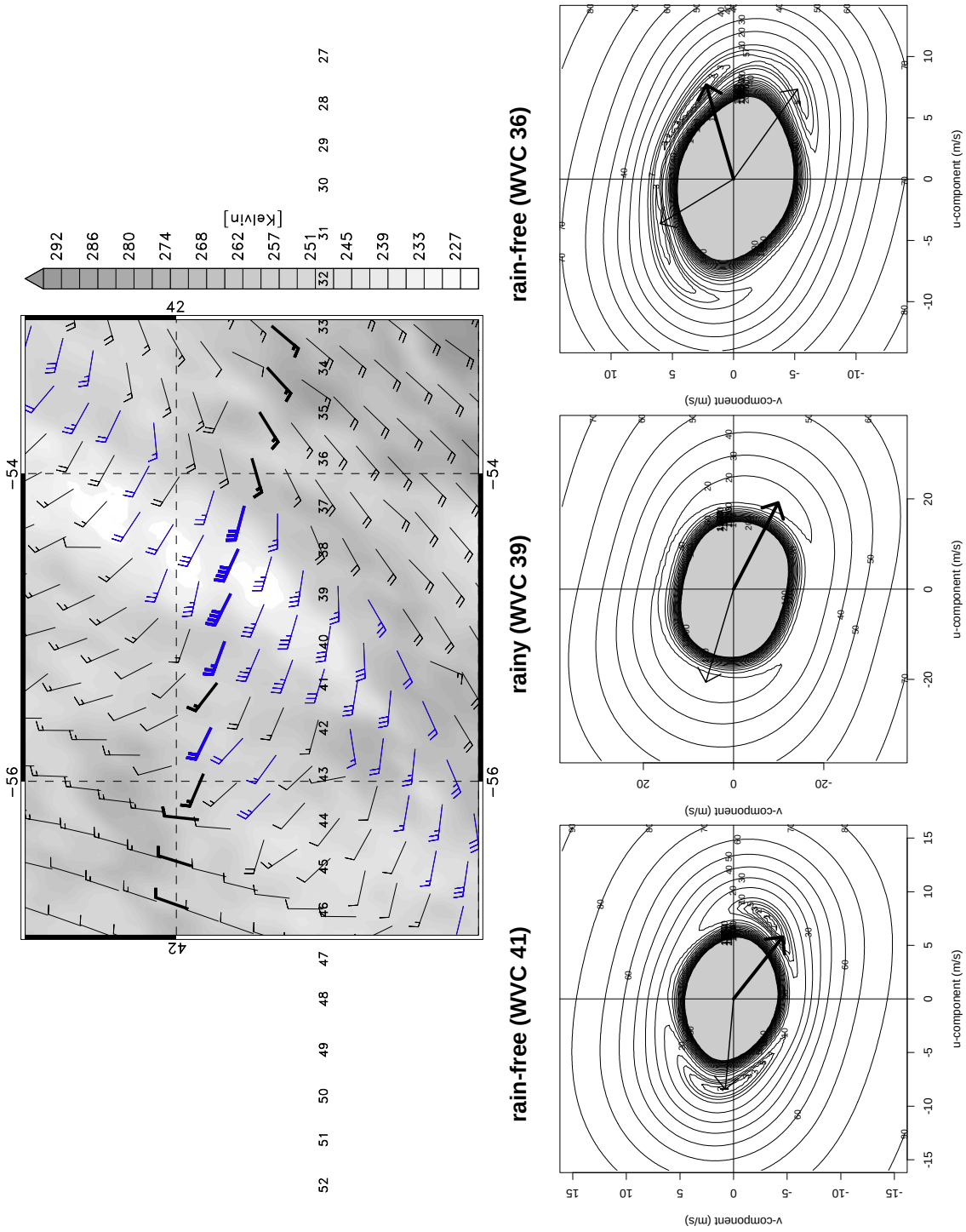

Assimilation of GOES Cloud Top Pressure Data into the Eta Model

Ying Lin[1], Geoff DiMego[1], Brad Ferrier[2], Jim Jung[3], Dennis Keyser[1], Eric Rogers[1]
[1]NCEP/EMC, [2]SAIC, Camp Springs, MD, USA
[3]CIMSS/U.Wisc, USA
Ying.Lin@noaa.gov

The hourly, 10-km cloud-top pressure data, derived from the GOES-8 and 10 sounder radiances, provide valuable information on the model fields above the cloud tops. We have conducted experiments to assimilate these cloud top data, mainly by using them to remove spurious cloud above the observed cloud top level, while making minimal adjustments to the moisture field at the level of observed cloud top.

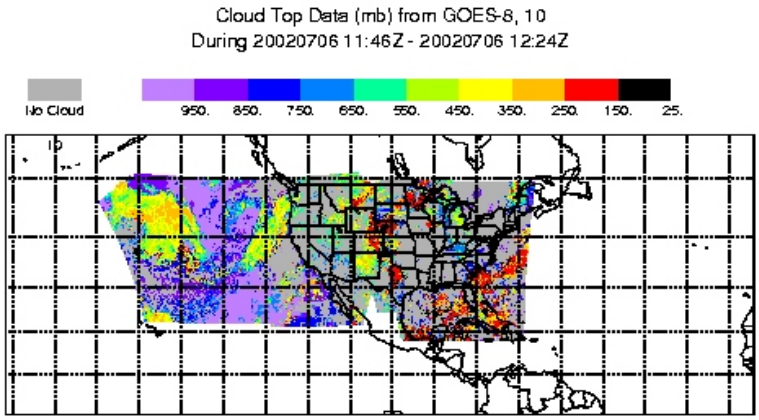

Fig. 1. An example of GOES cloud top pressure data

During the 12h pre-forecast data assimilation period, at each physics time step and for each horizontal grid point where a valid GOES cloud top observation is available, condensate (water or ice) is removed from the model above the GOES cloud top level (or removed from the entire column if the satellite data indicate that this point is cloud-free).The water vapor mixing ratio is also set to no more than grid-scale saturation (with regard to liquid water when the temperature is above -10 C, with regard to ice below -10 C). At the model level closest to the observed cloud top, if the air is subsaturated, then it is moistened at a rate that just brings it to saturation in one hour.

The cloud top assimilation has been tested on its own at 32km resolution (where the only difference between the test run and the control run is the addition of the cloud top data) and at 12km resolution, in combination with other planned upgrades for the Eta model (improved cloud physics and radiation, assimilation of radar radial winds *etc.*; - see http://wwwt.emc.ncep.noaa.gov/mmb/tpb.spring03/tpb.htm). The impact on precipitation forecasts (Fig. 2) and upper air fields (Fig. 3) has been generally positive. This package of upgrades to the Eta model is scheduled to be implemented during Spring/Summer 2003.

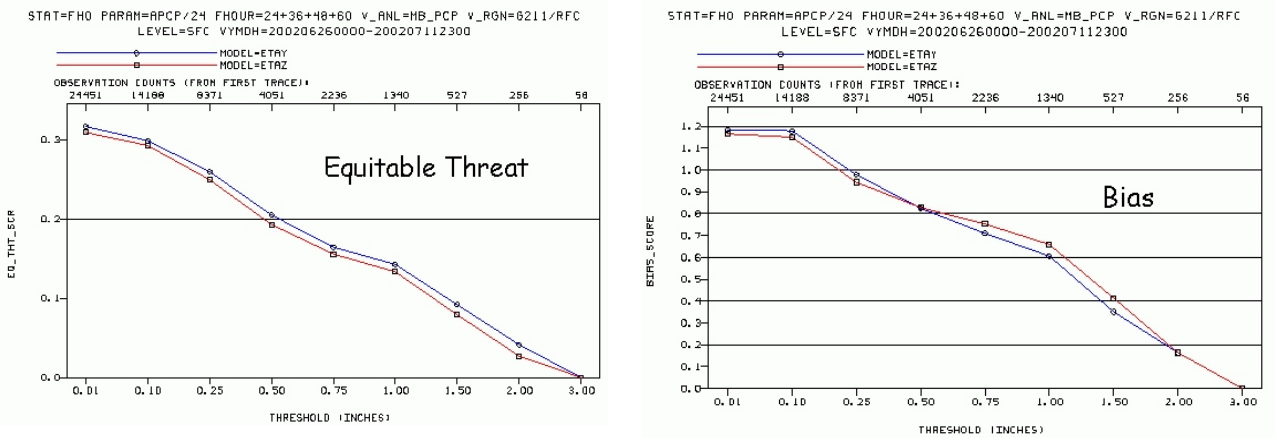

Fig.2 Equitable threat and bias scores of the 32km Eta parallel run (25 Jun - 9 Jul 2002), with cloud top assimilation (blue) and the control run (red), for 24+36+48+60h forecasts.

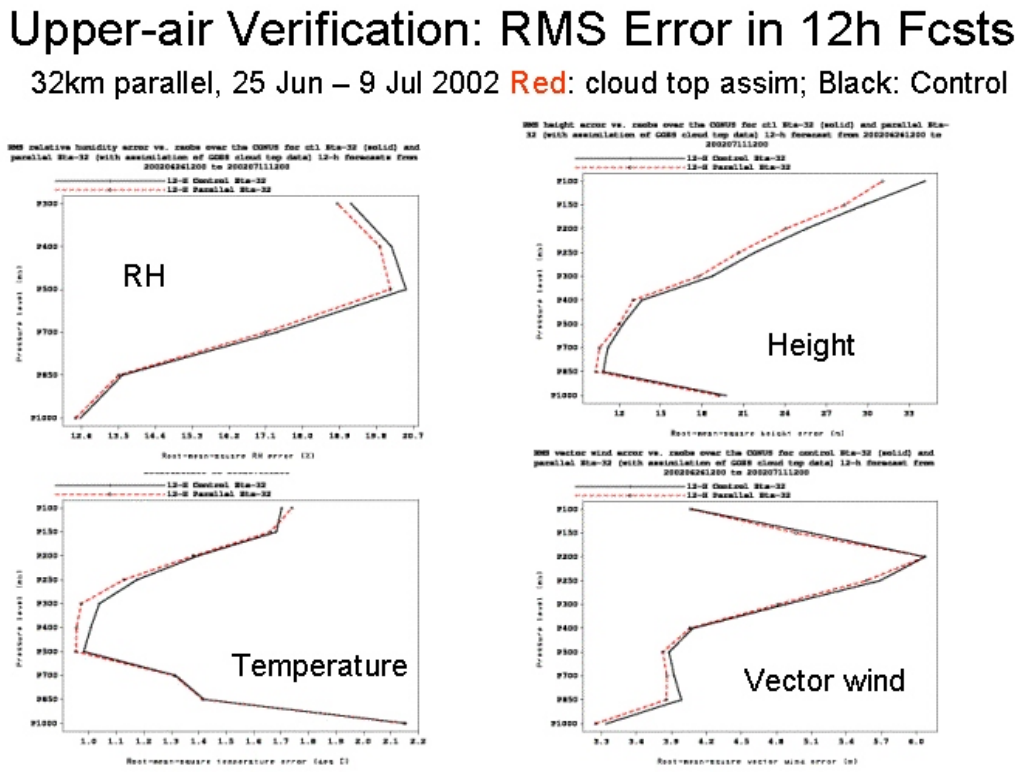

Fig.3 Upper-air verifications for the parallel run.

On the lower boundary condition of tangent-linear models

Jean-François Mahfouf and Stéphane Laroche

Meteorological Service of Canada, MRB/RPN
DORVAL, QC (Canada)
email address: jean-francois.mahfouf@ec.gc.ca

1 Introduction

A number of studies (Buizza, 1994; Janisková et al., 1999; Mahfouf, 1999) have shown that adiabatic tangent-linear (TL) versions of numerical weather prediction models produce too large evolved perturbations close to the surface when compared to pairs of non-linear (NL) model integrations (ranging between 6 and 48 hours). As a result, non-physical modes are generated in the computation of singular vectors and the convergence of 4D-Var can be affected when assimilating near-surface observations. This problem has been solved by including linearized vertical diffusion schemes in order to describe dissipative processes generated by turbulence near the Earth's surface. Simple schemes based on an analytical (and linear) formulation of the eddy exchange coefficients as the one proposed by Buizza (1994) are sufficient to make the TL model much more realistic in the boundary layer. More sophisticated schemes have been also been considered (Mahfouf, 1999; Laroche et al., 2002) but the strong non-linear dependence of the exchange coefficients with the basic flow can produce too large perturbations in the TL model that need to be filtered.

2 The lower boundary condition

One aspect that has not been examined in details up to now is the specification of the lower boundary condition. The turbulent flux F_ψ of a given prognostic variable ψ (wind, potential temperature, specific humidity) in the surface layer is expressed by the classical bulk formula:

$$F_\psi = K(\psi_L - \psi_s)$$

with $K = \rho C_D |U_L|$ where C_D is a drag coefficient depending upon static stability and surface roughness, U_L the wind speed at the lowest model level, ρ the air density. This flux is proportional to the gradient of ψ between the lowest model level Z_L and the surface Z_s.

For the momentum flux, the lower boundary in a TL model is obvious since the wind vanishes at the surface (i.e. $\psi_s = 0$), then for the wind perturbation: $\psi'_s = 0$. However, for potential temperature and specific humidity, the specification of model variables at the surface is more complicated.

The perturbed flux can reasonably be approximated by:

$$F'_\psi = K(\psi'_L - \psi'_s)$$

Moreover, when $K' \neq 0$ noise can appear in the TL model.

Over oceans, the surface boundary condition θ_s is specified from a sea surface temperature analysis and kept constant during the integration of the forecast model. Specific humidity, being equal to the saturation value, is also constant with time. This behavior of the NL model (i.e. $\psi_s = cst$) implies a similar boundary condition as for momentum in the TL model : $\psi'_s = 0$.

Over continents, θ_s evolves during the forecast according to the surface energy balance where the radiative forcing induces a strong diurnal cycle. Similarly, $q_s = \alpha q_{sat}(\theta_s)$, where α depends upon soil characteristics (soil moisture principally), has also strong diurnal variations. For these two quantities, imposing $\psi'_s = 0$ is not a reasonable assumption but it was nevertheless implemented at ECMWF and Météo-France for convenience. The consequence is a damping of the temporal evolution of near surface perturbations as shown recently by Trémolet (2003) and previously noticed by M. Janisková (personnal communication). To take into account the evolution of q'_s and θ'_s in a proper way one would need a linearized version of a land surface scheme and of a radiation scheme (including clouds). We propose here a simple solution that produces more realistic perturbations near the surface than when $\psi'_s = 0$ is imposed without having to consider additional linearized versions of physical processes.

In our proposal, we impose $\psi'_s = \psi'_L$ which corresponds to a zero perturbed flux (when $K' = 0$). It can also be interpreted as keeping the vertical gradient from the trajectory between the surface and the lowest model level.

3 Summary

In this short paper we are suggesting the following boundary conditions for application in TL numerical weather prediction models :

- $U'_s = 0$
- $\theta'_s = LSM \times \theta'_L$
- $q'_s = LSM \times q'_L$

where $LSM = 0$ over oceans and 1 over continents. This proposal has been tested in the TL version of the GEM model with a beneficial impact on the evolution of analysis increments for temperature and specific humidity in the planetary boundary layer.

4 References

Buizza, R., 1994: Sensitivity of optimal unstable structures. *Quart. J. Roy. Meteor. Soc.*, **120**, 429-451

Janisková, M., J.-N. Thépaut, and J.-F. Geleyn, 1999: Simplified and regular parameterizations for incremental four-dimensional variational assimilation. *Mon. Wea. Rev.*, **127**, 26-45

Laroche, S., M. Tanguay, and Y. Delage, 2002: Linearization of a simplified planetary boundary layer parameterization. *Mon. Wea. Rev.*, **130**, 2074-2087

Mahfouf, J.-F., 1999: Influence of physical processes on the tangent-linear approximation. *Tellus*, **51A**, 147-166

Trémolet, Y. 2003: Diagnostics of linear and incremental approximations in 4D-Var. ECMWF Technical Memorandum No 399, 16pp.

INTERCOMPARISON OF GLOBAL LAND SURFACE SOLAR INSOLATION IN OPERATIONAL GCMS

C. Jesse Meng
jesse@hsb.gsfc.nasa.gov
GEST, University of Maryland Baltimore County, Baltimore, Maryland 21250

Co-workers
P. R. Houser, K. Mitchell, M. Rodell, U. Jambor, J. Gottschalck, K. Arsenault, B. Cosgrove, J. Radakovich, M. Bosilovich, J. K. Entin, J. P. Walker, H. L. Pan, and G. Gayno

1. INTRODUCTION

Solar insolation absorbed at the Earth's surface is the primary forcing of the surface water and energy cycles. However, it is one of the most misrepresented variables in general circulation models (GCMs), due to the inaccuracy in modeled cloud structure and its variation. In a GCM, errors in surface radiation budget can lead to inaccurate simulations in surface temperature, soil moisture, surface heat fluxes, and consequently, the atmospheric circulation. This has motivated the development of a Global Land Data Assimilation System (GLDAS) (Rodell et al., 2003), which is collaboration between the National Aeronautics and Space Administration's Goddard Space Flight Center (NASA/GSFC) and the National Oceanic and Atmospheric Administration's National Centers of Environmental Prediction (NOAA/NCEP). The concept of GLDAS is taking a GCM-constructed land-atmosphere environment, and using an un-coupled land surface scheme, forced by observations, to produce optimal fields of land surface states and fluxes.

A 1/4 degree resolution GLDAS has been implemented in near real time, using various satellite- and ground-based observing systems. Currently, two operational GCMs, namely, the NASA/GSFC GEOS (Pfaendtner et al., 1995) and the NOAA/NCEP GDAS (Derber et al., 1991), are available in GLDAS to provide the baseline land-atmosphere environment. Surface solar insolation from the GCM is then replaced by an observation-based product to force GLDAS. The Air Force Weather Agency (AFWA) Real Time Neph-analysis (RTNEPH) is implemented, which is a global cloud analysis using geostationary and polar orbiting satellite observations. In RTNEPH, the observed cloud properties (cloud amount, type, and top and base heights) are reported every hour globally at a 24 km resolution. Surface downward shortwave and longwave fluxes are estimated from the observed cloud properties using the radiation scheme of the AFWA AGRMET model (Shapiro, 1987). In this study we evaluate the surface downward shortwave fluxes from the three models against ground observations. The main purpose is to understand the sources and feedbacks of the land surface water and energy cycles, thereby, contributing to the future development of land and atmosphere modeling and data assimilation systems.

2. EVALUATION OF SURFACE SHORTWAVE FLUXES

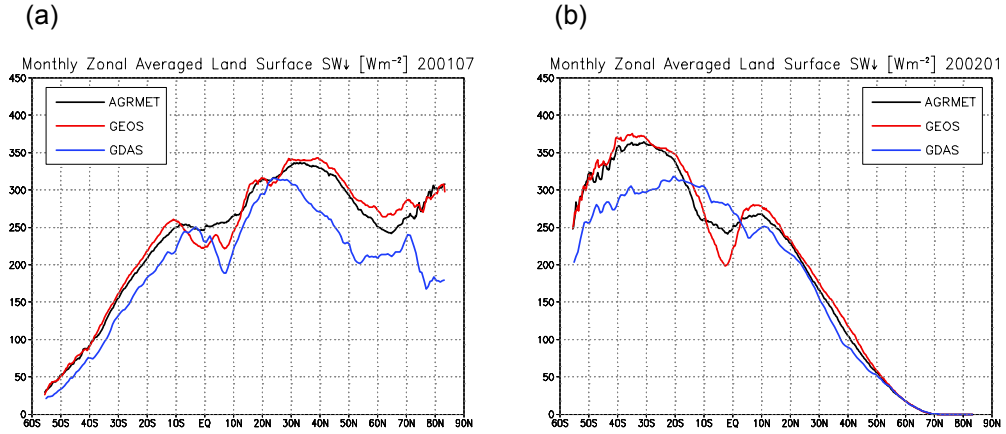

Figure 1. Monthly mean, zonal averaged, land surface downward shortwave fluxes for (a) July 2001, and (b) January 2002. Values are in Wm^{-2}.

Monthly mean, zonal averaged, land surface downward shortwave fluxes from the three models (AGRMET, GEOS, and GDAS) for July 2001 and January 2002 are shown in Figure 1. AGRMET and GEOS exhibit very similar patterns, except in the tropics. The differences in mid- and high-latitudes are within 10%. On the other hand, GDAS is about 10% lower than AGRMET in most of the winter hemisphere, and is about 20-25% lower in most of the summer hemisphere. Smaller spatial and temporal scale analysis indicates that the modeled fluxes are in a better agreement under clear-sky conditions, suggesting that the differences between the fluxes are attributed to the differences between the modeled (GEOS and GDAS) and observed (AGRMET/RTNEPH) cloud structures.

Monthly mean surface downward shortwave fluxes from the three models have been compared to the ground observations from the SURFRAD network. SURFRAD operates six sites over the continental United States to measure the surface radiation budget. The comparison results for July 2001 and January 2002 are summarized in Table 1. In general, AGRMET has an about 10% high bias in both summer and winter. The largest bias occurs at the site of Goodwin Creek, Mississippi (GWN) in January 2002. It is due to an underestimated fog effect, which has been improved in later experiments. Both GEOS and GDAS substantially overestimate (in percentage) surface shortwave fluxes in January 2002, suggesting that these two models underestimate the wintertime cloudiness.

(a) July 2001

SITE	SURFRAD	AGRMET	GEOS	GDAS
FPK	276	330	307	291
PSU	257	372	325	246
TBL	268	307	353	274
BON	275	313	269	274
DRA	340	346	362	331
GWN	257	273	256	260
BIAS		**10%**	**12%**	**0%**
RMS		**12%**	**17%**	**3%**

(b) January 2002

SITE	SURFRAD	AGRMET	GEOS	GDAS
FPK	55	58	77	72
PSU	74	78	102	83
TBL	104	99	133	121
BON	80	98	108	99
DRA	123	123	147	134
GWN	89	116	132	119
BIAS		**9%**	**33%**	**20%**
RMS		**15%**	**33%**	**20%**

Table 1. Comparison of modeled and observed surface downward shortwave fluxes at SURFRAD sites for (a) July 2001, and (b) January 2002. Values are in Wm^{-2}.

3. CONCLUSION

There is a large discrepancy between modeled land surface radiation budgets (up to 25%), due to the differences in modeled cloud structures. The impact of the different radiative forcing on the land surface water and energy cycles, namely, altering the surface heating, cooling, evaporating, and snow melting processes, will be investigated through the GLDAS experiments. Analyses on the European Centre for Medium-Range Weather Forecasts (ECMWF) output will be included in the future work.

REFERENCES

Derber, J. C., D. F. Parrish, and S. J. Lord, 1991: The new global operational analysis system at the National Meteorological Center. *Wea. and Forecasting,* **6,** 538-547.

Pfaendtner, J., S. Bloom, D. Lamich, M. Seablom, M. Sienkiewicz, J. Stobie, and A. da Silva, 1995: Documentation of the Goddard Earth Observing System (GEOS) Data Assimilation System - Version 1, *NASA Technical Memorandum 104606*, **4**, 44 pp.

Rodell, M., P. R. Houser, U. Jambor, J. Gottschalck, K. Mitchell, C. J. Meng, K. Arsenault, B. Cosgrove, J. Radakovich, M. Bosilovich, J. K. Entin, J. P. Walker, D. Lohmann, and D. Toll, 2003: The Global Land Data Assimilation System (GLDAS), *Bull. Amer. Meteor. Soc., accepted.*

Shapiro, R., 1987: A simple model for the calculation of the flux of direct and diffuse solar radiation through the atmosphere, *AFGL Scientific Report*, **35**, 40 pp.

On the use of BUFR-formatted AMVs from METEOSAT satellites

Kazuya Nojima[*1] and Yoshiyuki Nakamura[*2]
[*1](nojimak@msc.kishou.go.jp)
Meteorological Satellite Center, Japan Meteorological Agency
3-235 Nakakiyoto, Kiyose-City, Tokyo 204-0012 Japan
[*2](nakamura-y@met.kishou.go.jp)
Numerical Prediction Division, Japan Meteorological Agency
1-3-4 Otemachi, Chiyoda-Ku, Tokyo 100-8144 Japan

In order to cope with the format change of the AMVs (Atmospheric Motion Vectors) observed by the METEOSAT-5 and 7 from SATOB into BUFR form, quality investigation and the assimilation experiments were performed using ELW (Expanded Low Resolution) winds. According to the result of quality investigation, we confirmed that QI (Quality Indicator; added and reported to each wind vector in BUFR form) was effective to evaluate the quality of the data. The AMVs used in the experiments were changed from ELW (all imagers of IR (Infra-Red), VIS (Visual) and WV (Water-Vapor)) to ELW (IR), HRV (VIS) and HWW (WV) in April 2002. HRV and HWW winds have higher resolution than that of ELW winds. We performed the T106 global assimilation experiments with various options of QI utilization, and fixed the parameters to be preferable in the data assimilation processing in the operational NWP system. The preliminary test for the operational implementation with T213 global model was conducted for August 2002. The score is almost neutral but slight improvement was seen in the Southern Hemisphere. This scheme will be introduced in early FY2003.

Table: The QI utilization parameters for specified areas and vertical heights. The AMWs with higher QI than the values shown in the table are used in the data assimilation.

Area	Extra-tropical(20-60deg)			Tropical(0-20deg)		
height (hPa)	Low (~700)	Medium (700~400)	High (400~)	Low (~700)	Medium (700~400)	High (400~)
ELW (IR)	60	60	75	85	60	70
HRV (VIS)	60	-	-	60	-	-
HWW (WV)	-	-	90	-	-	70

The experiments of direct assimilation of ATOVS radicances in the JMA 3D-Var system

Kozo Okamoto, Masahiro Kazumori, Hiromi Owada
Numerical Prediction Division, Japan Meteorological Agency
1-3-4 Otemachi, Chiyoda-ku, Tokyo 100-8122,JANAN

email:okamoto@npd.kishou.go.jp,kazumori@met.kishou.go.jp,howada@naps.kishou.go.jp

1. Introduction

Since 1982, the Japan Meteorological Agency (JMA) has been operationally using the temperature profile data retrieved by NOAA/NESDIS. Currently, there are few observed information of atmospheric humidity in the JMA global analysis. The JMA uses radio-sonde-observed humidity profiles and statistically derived profiles from the Geostationary Meteorological Satellite (GMS-5) brightness temperature.

In 2000, the JMA operational system introduced a 1D-Var scheme of TOVS data in the 3D-Optimum Interpolation. In September 2001, the JMA introduced a 3D-Var data assimilation system in the operational global analysis. By using the 3D-Var assimilation system and a radiative transfer model, satellite radiances data can be assimilated directly without any conversion to analysis variable such as temperature or relative humidity.

2. Setting of experiments

In the experiments, ATOVS radiances were assimilated directly in place of retrievals, and no statistical humidity retrievals from GMS-5 were used. As the fast radiative transfer model, RTTOV-6 developed at ECMWF was used. The experiments were performed for December 2001 and July 2002. A new cumulus parameterization scheme of JMA global model (Nakagawa 2003) was used jointly.

3. Results

The experiments have demonstrated some positive impacts on forecast skills for the geopotential height at 500 hPa in the southern hemisphere and in the tropical region (Fig.1). The improvement of forecast skill in the former part of forecast period was remarkable. The forecast scores of the temperature at 850 hPa, wind speed at 250 hPa and sea level surface pressure were similarly good. The temperature profiles in the upper stratosphere and the global humidity field in the troposphere were also improved. The accuracy of initial fields of temperature and humidity were confirmed against the total precipitable water from SSM/I (Fig.2) and radio-sonde observation. We also got better results on the typhoon track prediction and the global monthly mean 24-hour rainfall. However, the anomalous change of temperature at some levels in the stratosphere and the concentration of rainfall in 6-hour forecast were seen. To solve these problem, we have some plans to improve the global model and bias correction scheme of ATOVS

brightness temperature.

This direct assimilation scheme of ATOVS radiances will be implemented in the JMA operational global data assimilation system in April 2003.

References

Okamoto, K., Takeuchi, Y., Kaido, Y. and Kazumori, M., 2002:Recent developments in assimilation of ATOVS at JMA, Tech. Proc. of 12th International TOVS Study Conference, Lorne, Australia 2 Mar. -27 Feb. 2002. (Submitted)

Nakagawa, M.,2003:Development of a cumulus parameterization scheme of the operational global model at JMA. CAS/JSC WGNE Res. Act. in Atmos. Ocea. Model.(Submitted)

RTTOV-6 SCIENCE AND VALIDATION REPORT 2000. Available from the NWP SAF web site.

Saunders, R., M. Matricardi and P. Brunel, 1998: An improved fast radiative transfer model for assimilation of satellite radiance observations. Q. J. R. Meteorol. Soc., 125, 1407-1425.

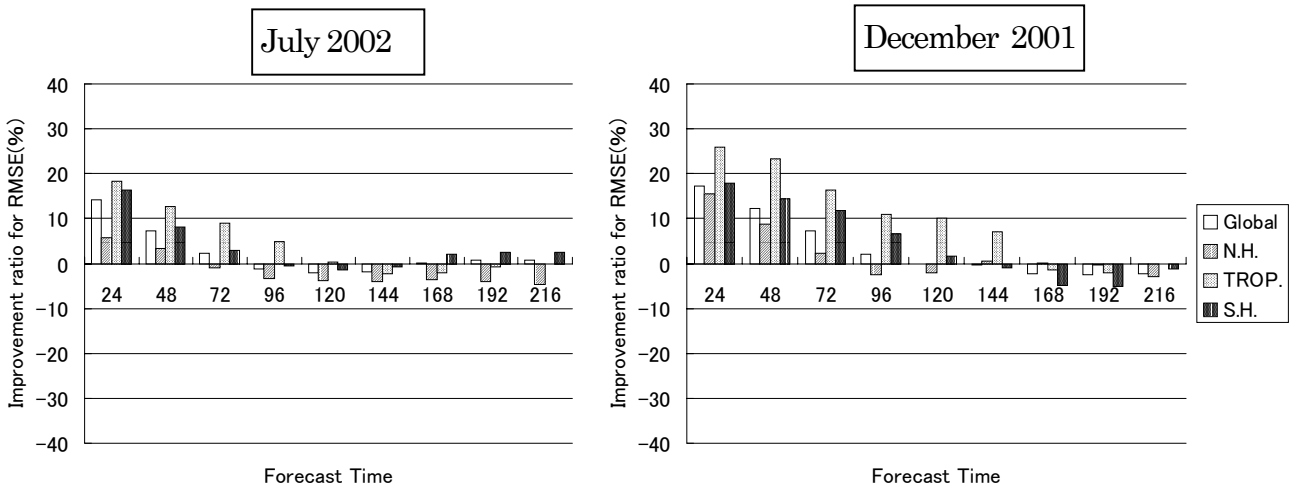

Fig.1: Improvement ratio for RMSE (%). Jul. 2002 (left) and Dec.2001 (right). Horizontal axis means forecast time in hours.

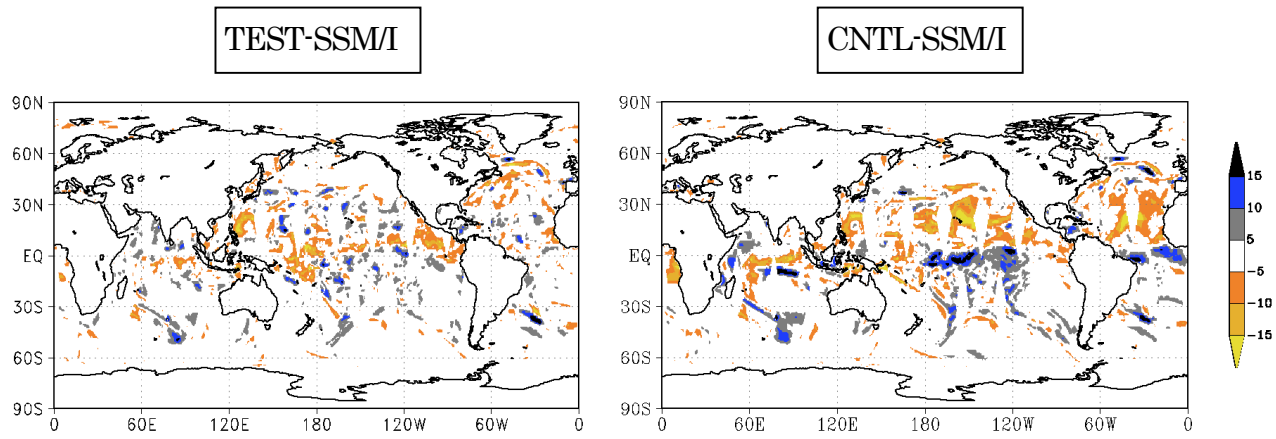

Fig.2: Differences of total precipitable water between the analyzed fields at 12UTC 1 July 2002 and SSM/I observation which is no assimilated. TEST-SSM/I (left). CNTL-SSM/I (right).

Modeling of Covariance Matrices by Generalized Diffusion Operators – A Hierarchical Approach

Andreas Rhodin (andreas.rhodin@dwd.de)
Deutscher Wetterdienst, Offenbach, Germany

March 13, 2003

Because of its size, the forecast error covariance matrix $\mathbf{P}^f$ for the model prognostic variables $\mathbf{x}$ is generally modeled by choosing a different set of control variables $\mathbf{v}$, related to $\mathbf{x}$ by a linear transformation, $\mathbf{x} = \mathbf{L}\mathbf{v}$, so that the error covariance matrix for $\mathbf{v}$ is simple (e.g., diagonal). Generally the matrix $\mathbf{L}$ is split into a balance operator $\mathbf{K}_b$ and a remaining operator $\mathbf{P}_u^{f\,1/2}$.

$$\mathbf{L} = \mathbf{K}_b \mathbf{P}_u^{f\,1/2} \tag{1}$$

$\mathbf{K}_b$ accounts for the correlations between variables by transforming unbalanced variables $\mathbf{x}_u$ into their balanced counterparts (for instance by considering the geostrophic balance equation). $\mathbf{P}_u^f$ represents the univariate spatial correlations and thus is a block-diagonal matrix with block matrices $\mathbf{C}_\eta$. η denotes the unbalanced variables of the model (temperature, humidity, vorticity, divergence). The square root of the correlation matrices, $\mathbf{C}_\eta$, may be represented by appropriate operators or filter functions, $\mathbf{C}^{1/2}$:

$$\mathbf{C}_\eta = \mathbf{C}_\eta^{1/2} \mathbf{C}_\eta^{T/2} \tag{2}$$

A common choice for $\mathbf{C}$ is a spectral transform [1], implying horizontally homogeneous and isotropic error covariance functions. This choice has serious limitations, because error covariances are flow dependent, and therefore their representation in data assimilation systems should be spatially varying. An alternative for representing $\mathbf{C}$ is to use digital filters in grid point space [2]. Digital filters can be implemented efficiently for Gaussian covariance functions on regular orthogonal grids by an alternating direction approach. An efficient application of both methods on an icosahedral grid, as used by the global model GME [3] of DWD, is difficult.

Weaver and Courtier [4] have proposed modeling the filter functions $\mathbf{C}_\eta^{1/2}$ by application of a diffusion operator, i.e. integrating the diffusion equation over a time span T starting with the unbalanced fields $\eta(\tau = 0)$, with

$$\frac{\partial \eta}{\partial \tau} - \bigtriangledown \kappa \bigtriangledown \eta = 0 \;, \tag{3}$$

This operator has been generalized in order to model non Gaussian correlation functions. Here a different generalization is proposed:

$$\frac{\partial \eta}{\partial t} - \bigtriangledown \kappa(\tau) \bigtriangledown \eta - c(\tau)\eta(0) = 0 \tag{4}$$

This formulation differs from (3) by the additional source term $c(\tau)\,\eta(0)$. For small values of τ, the coefficient $c(\tau)$ controls the shape of the correlation function on the large scales (long integration times $T{-}\tau$ of the diffusion equation), whereas for large values of τ (small $T{-}\tau$), it controls the shape on the fine scales. By choosing negative values of $c(\tau)$ for $\tau << T$ and positive values for $t \approx T$, correlation functions that are negative on the large scales can be modeled. By choosing anisotropic diffusion coefficients κ, anisotropic correlation functions are obtained.

The number of steps required to integrate equations (3) or (4) numerically is limited by stability criteria. However, the diffusion equation can be integrated efficiently using a multi-grid approach, by starting the integrating of equation (4) on a coarse grid for $\tau << T$ and then moving to finer grids for $\tau \approx T$. In praxis the algorithm is as follows:

1. Average the field $\eta(0)$ to the coarser grids.
2. Integrate the diffusion equation on the coarsest grid for a few (large) steps.
3. Interpolate the intermediate result to the next finer grid.
4. Integrate the diffusion equation for a few (smaller) steps. In practice the coefficients $c(\tau)$ and $\kappa(\tau)$ may be kept constant on each grid i, denoted c_i and κ_i.
5. Repeat steps 3 and 4 until the finest grid is reached.

Correlation functions of various shapes may be approximated by a linear combination of the filter functions y_i with appropriate coefficients c_i. The approach was tested on a 2-dimensional regular grid and is illustrated below. In this example 8 grids were used (with grid spacing differing by a factor of 2) until the coarsest grid was reached (one grid point only).

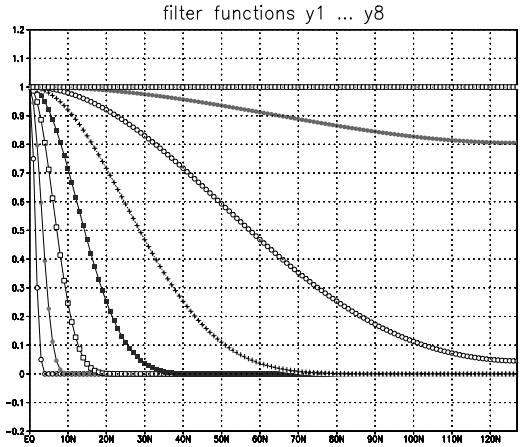

a) Filter functions y_i obtained by setting $c \neq 0$ on grid level i only.

b) Gaussian correlation function approximated by a linear combination of the functions $y_1 \ldots y_8$.
open circles: specified covariance function $\exp(-r^2/l^2)$
crosses: correlation function obtained by applying the approximated filter function.
filled circles: required filter function (square root of the above covariance function).
open squares: approximated filter function.
filled squares: difference of the exact and approximated filter function.

c) As b), but for a covariance function
$c = (\cos(rl_c) + sin(rl_c)/(ll_c))\exp(-r/l)$.

Up to now the multi-grid approach was motivated by the goal to yield an efficient operator representation of the filter functions. The approach may be modified by defining not only the coefficients c_i on the hierarchical grid, but the control variables $\mathbf{x}_i$ as well. Then, the control variables are representing analysis increments on different scales at different locations, and the transformation $\mathbf{L}$ behaves like a wavelet transformation.

References

[1] J. Derber and F. Bouttier. A reformulation of the background error covariance in the ECMWF global data assimilation system. *Tellus*, 51A(2):195–221, 1999.

[2] X.-Y. Huang. Variational analysis using spatial filters. *Mon. Wea. Rev.*, 128:2588–2600, July 2000.

[3] D. Majewski, D. Liermann, P. Prohl, B. Ritter, M. Buchhold, T. Hanisch, G. Paul, W. Wergen, and J. Baumgardner. *Mon. Wea. Rev.*, 130(2):319–338, Feb. 2002.

[4] A. T. Weaver and P. Courtier. Correlation modelling on the sphere using a generalized diffusion equation. *Q. J. R. Meteorol. Soc.*, 127:1815–1846, 2001.

Data Assimilation for Convective Scale NWP

Ian Roulstone
Met Office, JCMM, Meteorology Building,
University of Reading, Reading RG6 6BB. U.K.
ian.roulstone@metoffice.com

1 Preliminary work with the Unified Model

The performance of the next generation of very short range forecast system, will depend, in part, on the ability to assimilate observations, especially of precipitation, cloud and fog, with frequent updates. Current and future variational techniques available in the Met Office's Unified Model (UM) system form a sound basis for this, but high resolution and speed requirements bring additional challenges in formulation and performance. The performance of the current Latent Heat Nudging techniques may be very different when convection is partially resolved, and alternative approaches may be needed. Since any convective scale system would be closely coupled to lower resolution (mesoscale) NWP, the performance of the lower resolution system is crucial. A strategy is needed which optimises short range performance and timeliness which may be a combination of different analysis resolutions, update cycles, and techniques (e.g. 4D VAR, 3DVAR and nudging). This strategy needs to be both pragmatic and based on a clear understanding of the assimilation process. At present, we have insufficient information on the potential performance of current and planned technology to formulate proposals for future developments. Our current work is therefore aimed at furnishing this information.

Some of the research will be carried out as part of a collaborative programme on storm scale forecasting between the Met Office groups at the Joint Centre for Mesoscale Meteorology and various groups within the university community. Research projects investigating the assimilation of precipitation data, including Doppler radar, the improvement of the conditioning of the control variable transforms and the inclusion of boundary layer forcing, are being carried out by postgraduate and postdoctoral researchers at the universities of Reading, Essex and Salford (as part of the Universities Weather Research Network).

Once the NWP system is able to capture adequately the state of existing systems (such as convective storms) in its analysis, substantial improvements to very short range forecasts of development should result. This development work is an essential prerequisite.

Our goal is to identify an optimal strategy, given existing assimilation technology, for data assimilation for high resolution models. Validation of the performance of the system against, especially, routine and research radar observations will be undertaken. A literature survey of progress in related areas has been carried out by Dance (2003).

An initial assessment of the performance of the convective scale model initialised with various reconfiguration strategies is underway, and we have started to run 3DVAR at 4km horizontal resolution. Increments are being added via an incremental analysis update procedure, and preliminary results are encouraging.

2 Moisture flux convergence and precipitation

We are investigating a new approach to the assimilation of radar precipitation data into mesoscale, and ultimately, convective scale models. The new approach is based on a strategy in which the model's wind, temperature and humidity fields are adjusted in response to the perceived error in model's representation of moisture flux convergence. The new assimilation scheme will be tested using the high-resolution version of the current mesoscale model that is being developed by the Met Office group at the JCMM in Reading. Tests show that this can be run at 2km resolution with a one-minute time step and produces realistic rainfall fields. The high resolution means that convective precipitation is more likely to be explicitly resolved, rather than being parameterised as occurs in the present 12km operational model.

Our current knowledge of atmospheric water balance suggests the following simple model relating aerodynamic moisture flux to surface precipitation under conditions where surface exchanges

are of negligible importance:

$$P = -\alpha \int \mathrm{d}\sigma(\nabla_h.(\mathbf{v}\rho_\nu)) + \epsilon, \tag{1}$$

where P is either the model or 'observed' precipitation rate over a model grid box; α is some unknown constant of proportionality, $\mathbf{v}$ is horizontal wind velocity, ρ_ν is absolute humidity, ϵ is a residual error resulting from the approximations employed, and σ is the vertical coordinate.

The flux convergence term can be decomposed to represent the influence of convergence and advection, and if the contribution of the divergent part of $\mathbf{v}$ in the advection is small, we have

$$-\int \nabla_h.(\mathbf{v}\rho_\nu)\mathrm{d}\sigma = -\int \rho_\nu \nabla_h.\mathbf{v}_\chi \mathrm{d}\sigma - \int \mathbf{v}_\psi.\nabla_h \rho_\nu \mathrm{d}\sigma.$$

According to Robertson (1999), the dominant contribution is from the kinematic convergence term, at least on the scale of a single model grid box. Such a result suggests a simple variational adjustment strategy, involving only changes to ρ_ν and $\mathbf{v}_\chi$ on the model grid subject to the constraint that the adjusted total convergence is consistent with observed precipitation rates according to (1).

However, such an adjustment does not necessarily result in an adjusted state that lies on the slow manifold of the model. An alternative approach is to relate P to the *vertical humidity flux*, by making the approximation

$$-\int \nabla(\mathbf{v}\rho_\nu)\mathrm{d}\sigma = w\rho_\nu,$$

where w is vertical velocity at some model level. It is possible to express w as the solution of a suitable balance equation which expresses the divergent motion in terms of the model's prognostic variables. This methodology is to be used as the basis of a 'forward model' relating incremental variations in P to incremental variations in the prognostic variables. Equation (1), and the approximations discussed, can be used to derive a tangent linear model to predict the variation in P in response to the model wind, temperature and humidity variables. An important feature of this approach is that it implies some impact on the model analysis in *any* region where observed and predicted precipitation rates differ.

The first stage has been to confirm the relationship between the precipitation and the moisture flux convergence as resolved by the high resolution model. This work has been completed and we are now adapting 3DVAR to modify the model analysis so that the diagnosed moisture flux convergence into each model grid box is consistent with that implied by the co-located precipitation rate observed by the radar. The impact of the scheme on mesoscale forecasts will be evaluated at various resolutions and the sensitivity to errors in the radar derived rainfall examined.

References

Dance, S.L. (2003) Issues in high resolution limited area data assimilation for quantitative precipitation forecasting. Forecasting Research Technical Report 420, Met Office, UK.
http://www.metoffice.com/research/nwp/publications/papers/index.html

Robertson, N. (1999) Predictability of catchment-scale frontal precipitation using atmospheric moisture budget theory. *MSc dissertation, University of Reading, U.K.*

DATA ASSIMILATION EXPERIMENTS IN NERIMA HEAVY RAINFALL
- HOW USEFUL ARE DOPPLER RADAR RADIAL WIND AND GPS-DERIVED WATER VAPOR? -

Hiromu Seko[(1)], Takuya Kawabata[(1)], Tadashi Tsuyuki[(1)],
Hajime Nakamura[(2)], Ko Koizumi[(2)], Tetsuya Iwabuchi[(3)]

[(1)] Meteorological Research Institute, Japan Meteorological Agency, Tsukuba, Japan
[(2)] Numerical Prediction Division, Japan Meteorological Agency, Tokyo, Japan
[(3)] Japan Society for the Promotion of Science, Meteorological Research Institute, Tsukuba, Japan

1. Introduction

In summer, the thunderstorms that developed in the urban area sometimes cause the heavy rainfall. The generation and development of the thunderstorms are affected by the low-level convergence and the moist air supply. Radial wind (RW) data from Doppler radars and water vapor data from GPS (Global Positioning System) ground receivers are useful for capturing mesoscale wind and moisture fields, respectively. However, their benefits for mesoscale numerical weather prediction have not been well demonstrated so far.

In this study, to investigate the impacts of the RW that was observed by two Doppler radars and the GPS-derived water vapor, data assimilation experiments on the heavy rainfall event that occurred in Tokyo on 21 July 1999 (Nerima heavy rainfall) were performed by the 4-dimensional variational data assimilation (4d-Var DA) system for the Mesoscale model of the Japan Meteorological Agency (JMA). RW is expected to have a great impact, because it can provide the information of the horizontal wind in the small precipitation region where the horizontal wind can not be retrieved by the simplified VVP method and so on. The GPS-derived water vapor data used in this study are PWV and Slant water vapor (SWV). SWV is the water vapor amount from the GPS satellite and GPS receivers. Because the slant path of this data contains the information of the three dimensional distribution of water vapor, it is expected that the moist air supply at lower levels will be better reproduced by assimilating SWV data.

2.'Nerima heavy rainfall'

On 21 July 1999, the Baiu front crossed the northern part of the Japan and moved southward slowly. On the southern side of the Baiu front, the convections that had a scale of several ten kilometers were generated at the northeastern part of the Kanto area (the central part of the Mainland of Japan) at 15JST. The convections moved southeastward, and the intense hourly precipitation of 111.5 mm/hour was observed at Nerima, Tokyo at about 16JST. When the intense convections were developed, the easterly and northerly flows were generated in the precipitation regions (Fig.1). These flows and the southwesterly inflow from the south converged on the southern edge of the precipitation regions. Although this precipitation began to decay from 17JST, it lasted until 21JST over the southern part of the Kanto area.

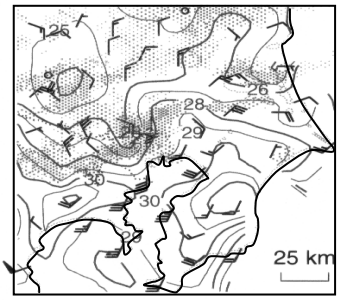

Fig.1 Horizontal distribution of precipitation region (shade), surface temperature (solid line) and horizontal wind at 16JST 21 July 1999.

3. Results of the data assimilation experiments

The precipitation regions moved southward, and came into the observation ranges of the Doppler radars at 15JST. Thus, the assimilation of the RW of the Doppler radars and GPS-derived water vapor was performed with the data from 9JST to 15JST. The analyzed fields at 15JST that were estimated by 4d-Var DA were used as the initial conditions of the numerical prediction. The impacts of the data assimilation of RW, PWV and SWV were investigated by comparing with the predicted hourly precipitation from the analyzed fields of 15JST and the observed one.

When the assimilation was not performed, no precipitation region was generated at the southern part of the Kanto area (Fig. 2a). When the conventional meteorological data was assimilated (Fig. 2b), the southeasterly flow in the precipitation region was reproduced. However, it did not last for long time. The scattered small precipitation regions were generated in the mountainous region far from Tokyo, and no precipitation region appeared at the Kanto area.

When PWV or SWV data was assimilated (Fig. 2c or 2d), the low-level inflow became more humid. The humid inflow generated the precipitation along the low-level convergence zone. However, in both experiments, the position of the precipitation was shifted eastward from the observed one. It is evident that the precipitation regions coincided with this convergence zone. The error of the precipitation position was due to the inaccurate prediction of the wind fields. When the RW was assimilated (Fig. 3a), the northerly wind was reproduced at the northwest of Tokyo. Because the northerly flow intensified the low-level convergence, the precipitation region was generated. The position of this precipitation region was almost the same as the observed one. However, the generation of the precipitation was delayed by one hour, because the low-level inflow from the south was less humid than the observed one.

When GPS-derived water vapor and RW were added to the assimilation data simultaneously (Figs. 3b and 3c), there were large improvements in the position and extent of the

*Corresponding author address: Hiromu Seko
Meteorological Research Institute,
1-1, Nagamine, Tsukuba, Ibaraki, 305-0052, Japan,
e-mail:hseko@mri-jma.go.jp

precipitation region. In both experiments, the positions of the predicted precipitation regions were closer to that of the observed one. In addition, the extent of the precipitation region increased substantially. This is due to the changes in the wind field. The assimilation of RW data produced the northerly flow northwest of Tokyo, which intensified a low-level convergence. This convergence generated the precipitation where the observed heavy rainfall occurred. This precipitation lasted until 21JST (FT=6hour), and the position and extent of the precipitation region were well predicted until 21JST.

The benefit of SWV data was also investigated by comparing the vertical distribution of water vapor. On the inflow side of the heavy rainfall (i.e. southern side), the water vapor above the height of 1km was reduced when SWV data was assimilated (Fig.4). The lower-layer water vapor was also reduced when PWV data was assimilated. The vertical water vapor distribution of the former experiment was more realistic, although the positions and appearance times of the precipitation regions were almost the same.

4. Summary

The assimilation of RW data of the Doppler radar and GPS-derived water vapor data was performed and their impacts on the prediction of the precipitation were investigated. When both data were used as the input data of 4d-Var DA, the prediction of the precipitation was improved significantly. It was also shown that the SWV data has the potential of the reproduction of the vertical structure of the water vapor. In order to confirm the impact of SWV data, a further study is needed with more number of rainfall events.

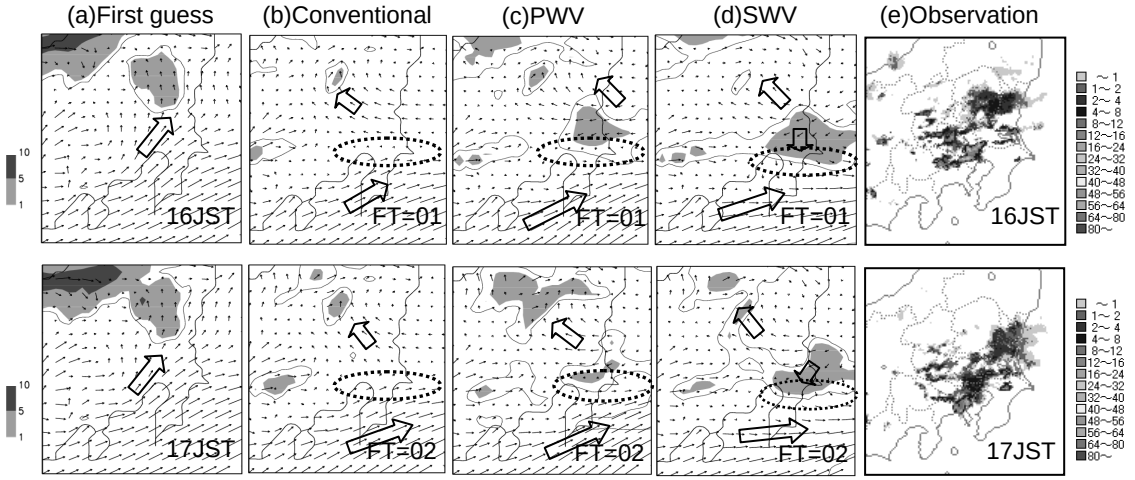

Fig. 2 Prediction of hourly precipitation and horizontal wind at 0.5 km from 15JST, July 21, 1999. Upper row is 1 hour forecast valid at 16JST and lower row is 2 hour forecast valid at 17JST. From left to right columns are (a) the first guess fields, (b) prediction from 4d-Var DA of the conventional data (rawinsonde etc), (c) prediction from 4d-Var DA with PWV added, (d) prediction from 4d-Var DA with SWV added, and (e) the rainfall intensity observed by JMA radars. Contour lines indicate hourly precipitation and arrows are horizontal wind at 0.5 km. Large arrows show major flows.

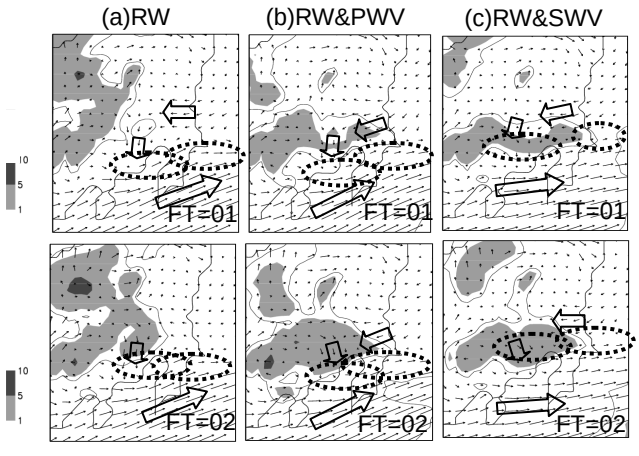

Fig. 3 Same as Fig. 2 but for, (a) prediction from 4d-Var DA with RW added, (b) prediction from 4d-Var DA with PWV and RW added and (c) prediction from 4d-Var DA with SWV and RW added from left to right columns.

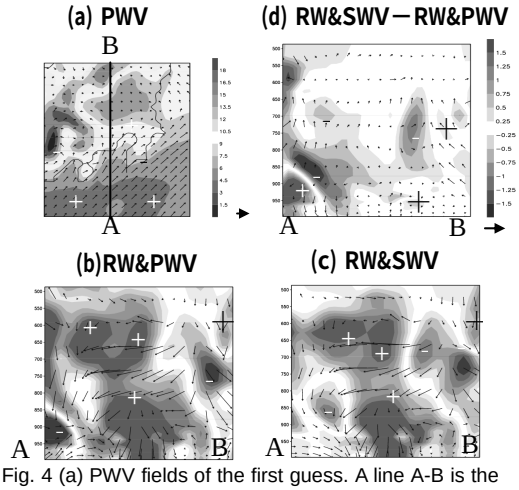

Fig. 4 (a) PWV fields of the first guess. A line A-B is the position where cross sections cut across. (b) and (c) are vertical cross-sections of the difference of specific humidity of 'RW&PWV' and 'RW&SWV' from the first guess. (d) is the vertical distribution of the difference between these experiments.

Adjoint of the non-hydrostatic GEMDM LAM

Monique Tanguay
Meteorological Service of Canada, Dorval, Québec, Canada
Email: monique.tanguay@ec.gc.ca

GEMDM refers to the distributed memory version of the Global Environmental Multiscale (GEM) model (Côté *et al.*, 1998) used operationally at the Canadian Meteorological Centre. The non-hydrostatic version is also available (Yeh *et al.*, 2002). Recently, GEMDM was also configured for limited area modelling (LAM) (Desgagné and Lee, 2003). On the assimilation side, work are currently in progress to extend the 3D-Var system (Gauthier *et al.*, 1999) to a 4D-Var system (Gauthier *et al.*, 2002). This has requested the coding of the adjoint of the first version of GEMDM. Recently, this coding has been extended to the new capabilities of GEMDM i.e. its non-hydrostatic and LAM aspects. Detailed experiments are planned for the coming year.

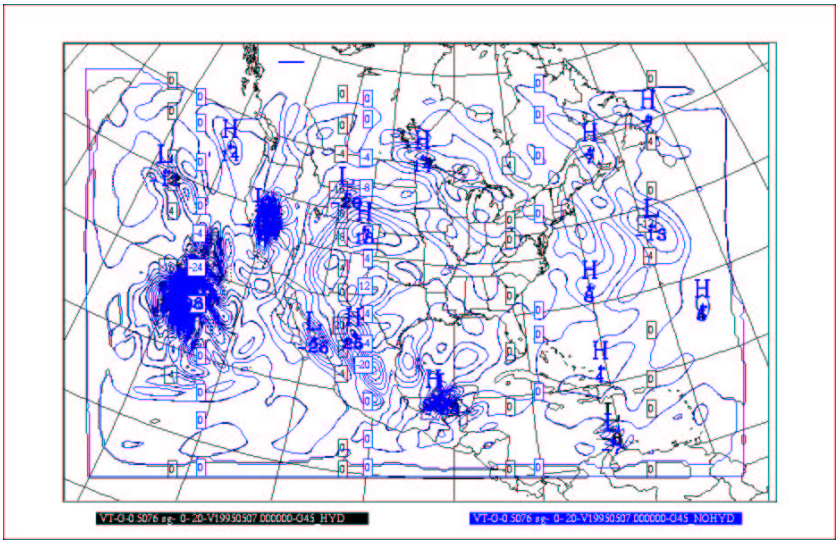

Fig: Superimposed hydro. and non-hydro. adjoint VT, 500 hPa, $dx = .45°$, after $t = 4$ hr.

References

Côté J., S. Gravel, A. Méthot, A. Patoine, M. Roch, and A. Staniforth, 1998: The operational CMC-MRB Global Environmental Multiscale (GEM) model: Part I - Design considerations and formulation, Mon. Wea. Rev. 126, 1373-1395.

Gauthier P., M. Tanguay, S. Pellerin, N. Ek, S. Laroche, and J. Morneau, 2002: Current status of the pre-operational 4D-Var assimilation system at MSC, 5th Workshop on Adjoint Applications in Dynamic Meteorology, Mount Bethel, Pennsylvania, April 2002.

Gauthier P., C. Charette, L. Fillion, P. Koclas, and S. Laroche, 1999: Implementation of a 3D Variationa l data assimilation system at the Canadian Meteorological Centre. Part I: The global analysis, Atmosphere-Ocean, Vol. XXXVII, No.2, pp . 103-156.

Yeh, K.-S., J. Côté, S. Gravel, A. Méthot, A. Patoine, M. Roch, and A. Staniforth, 2002: The CMC-MRB global environmental multiscale (GEM) model. Part III: Nonhydrostatic formulation, Mon. Wea. Rev., 130, 2, 339-356.

Assimilation of QuikSCAT / SeaWinds Ocean Surface Wind Data into the Global Data Assimilation System at JMA

Masami Tokuno and Yasuaki Ohhashi
Numerical Prediction Division, Japan Meteorological Agency
1-3-4 Otemachi, Chiyodaku, Tokyo 100-8122, Japan
e-mail: tokuno@met.kishou.go.jp, ya-ohashi@met.kishou.go.jp

The Japan Meteorological Agency (JMA) used the ERS-2 scatterometer winds and surface pressure retrieved from the ERS-2 winds together with auxiliary data for the global analysis in the optimum interpolation scheme (OI) from July 1998 to January 2001.

The QuikSCAT satellite, a successor of ERS-2, was launched being equipped with a new scatterometer SeaWinds in June 1999. A large contribution to numerical weather prediction (NWP) is expected, as the width of QuikSCAT observation is more than three times wider than that of ERS-2 scatterometer. Taking an advantage of QuikSCAT winds, an observation system experiment (OSE) for QuikSCAT winds in July 2000 was conducted with the same assimilation method as that used for ERS-2 data. Results showed that QuikSCAT winds after the ambiguity removal and quality control performed at JMA had almost the same accuracy as ship or buoy data.

JMA introduced a three-dimensional variational scheme (3D-VAR) instead of OI to the global data assimilation system in September 2001. Using QuikSCAT winds in July 2000, an impact study was performed with the JMA 3D-VAR using T106L40 version of the JMA global NWP model. The results showed a large improvement over the Southern Hemisphere and a small or a neutral improvement over the Tropics and the Northern Hemisphere.

To use QuikSCAT Winds operationally with the JMA 3D-VAR, impact studies using QuikSCAT winds in December 2001 and July 2002 are performed with the T213L40 version of the JMA global NWP model.

The impact of all elements to model's performance is neutral in December 2001. However, obvious improvement is indicated in Mean Error of altitude for 850 hPa and 500 hPa in tropical regions (20N – 20S). Figure 1 shows Mean Error of altitude for 850 hPa in four regions (global (GL), northern hemisphere (NH, 20N – 90N), tropical region (TR, 20N – 20S), southern hemisphere (SH, 20S – 90S)), for TEST and CNTL. Mean Error of altitude in 850 hPa in TEST is extremely improved after 3 forecast days and becomes almost zero at 9 forecast days in the tropical region.

In July 2002, impact of almost all elements to model's performance is neutral as the same as in December 2001. Small decrease of RMSE in the Northern Hemisphere is appeared in temperature and altitude in 850 hPa and temperature in 500 hPa. Obvious improvement is indicated in Mean Error of temperature for 500 hPa in the Southern Hemisphere shown in Figure 2.

Figure 3 shows Anomaly Correlation of altitude for 500 hPa in the Northern Hemisphere in July 2002. Anomaly Correlation in TEST is extremely improved after 6 forecast days.

Furthermore we performed the experiment for the impact of the typhoon track forecast in July 2002. Figure 4 shows the forecast track of typhoon 7 (HALONG). QuikSCAT wind data were assimilated in the global model 6 hourly and the result of the forecasted track of typhoon from the initial time 12 UTC July 10 2002 is shown in Figure 4. Each line shows the best track, TEST, CNTL, ROUTINE, respectively. The error of forecasted typhoon track in TEST decreases about 100 km to the best track. Thus QuikSCAT wind data is effective to improve the forecast of typhoon track. Additionally, we performed statistics of the error of typhoon track forecast in 36 cases during July 2002. The result shows that the error of typhoon track forecast in TEST is extremely decreased after forecast time 72 hours in comparison with the other cases.

Throughout the experiment, QuikSCAT data were recognized to have a good enough quality to be used for NWP. The evident positive impacts were not recognized over all regions, but small positive impact over the Northern Hemisphere in summer. In addition, the remarkable positive impacts were recognized for typhoon track forecast. As the result, JMA will start to use QuikSCAT wind data in NWP operationally in early FY2003.

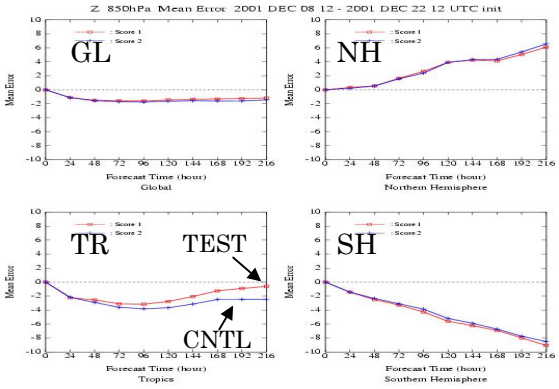

Figure 1 Mean Error of altitude for 850 hPa in December 2001.

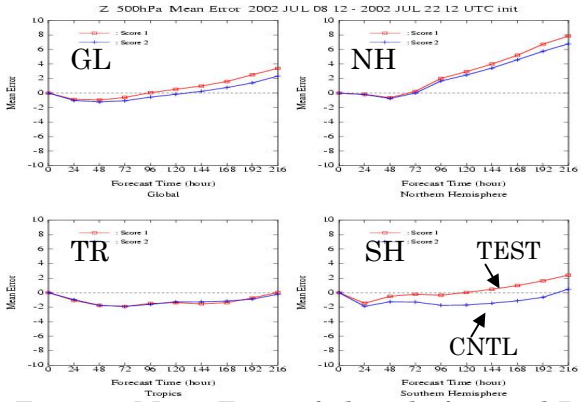

Figure 2 Mean Error of altitude for 500 hPa in July 2002.

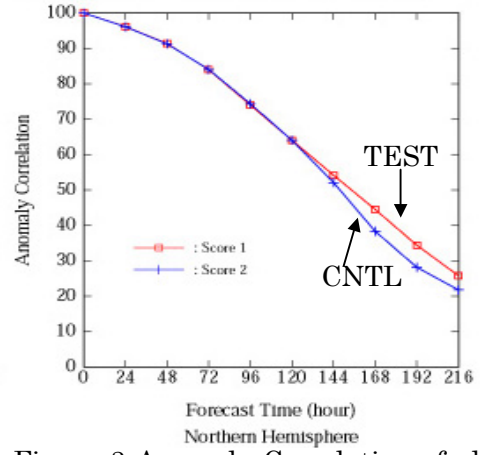

Figure 3 Anomaly Correlation of altitude for 500 hPa in northrern hemisphere in July 2002.

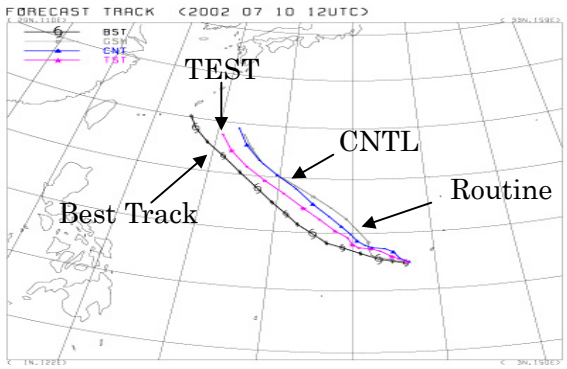

Figure 4 The results of forecast track of typhoon 7 (HALONG).

THE IMPACT OF TROPICAL RADIOSONDE DATA ON THE ARPEGE ANALYSES AND FORECASTS

M. Tounkara[1], P. Caille[2], and J. Pailleux[2]

1. INTRODUCTION

An Observing System Experiment (OSE) has been performed in order to evaluate the impact of the tropical radiosonde data on the meteorological analyses and forecasts. The data assimilation and forecasting system which has been used for this impact study is a particular version of the Météo-France operational ARPEGE system. Two parallel data assimilation suites have been run from 1 to 20 June 2000: one contains all the observations which are normally used operationally; the second one excludes all the TEMP and PILOT messages which are available in the tropical belt (20N-20S). From 00UTC, every day, forecasts are run from the analyses performed with and without the tropical radiosondes. The forecast pairs are then systematically compared over the whole globe through statistical scores as well as through synoptic map evaluation.

The general impact of the global radiosonde network on Numerical Weather Prediction (NWP) has been evaluated through several OSEs in the past (see WMO, 2000). Also, several regional studies have been performed to see the impact of modifications of the radiosonde network over the North Atlantic, Europe or North America. However no radiosonde impact study has been run which is specifically dedicated to the tropics. The atmospheric dynamics inside tropics is very different from mid-latitudes. Wind observations are known to be more important than mass observations near the equator to describe the dynamics, and the radiosonde network (TEMP plus PILOT messages) is the only system providing wind profile observations. In addition, the current radiosonde network is quite sparse between 20N and 20S: during the period 1-20 June 2000, around 70 TEMP observations are available at 00UTC and around 80 at 12UTC; none are available at 06 and 18UTC; 30 to 80 PILOT messages are available at each synoptic time: 00, 06, 12 and 18UTC. Out of the 70 or 90 TEMP observations available in this tropical belt, 50% are actually made on the area between 100E and 160E (South-East Asia to Australia), which represents one sixth of the surface.

The present experiment is one OSE recommended by the WMO Expert Team on the Observation Data Requirements and the Redesign of the Global Observing System. The goals are:

- to understand how the current tropical radiosonde network is important for the tropical analyses and forecasts;
- to understand how this observing system is important for the forecast in mid-latitude areas (i.e. how the information propagates from the tropics to mid-latitudes in the forecast);
- to get ideas for optimising the upper-air conventional network in the tropics.

2. THE ARPEGE ANALYSIS AND FORECASTING SYSTEM

The ARPEGE model is a global spectral model which has been developed in cooperation with ECMWF. In Météo-France operations, it is run with a variable mesh (stretched coordinate). For this OSE, the variable mesh option is not used, and the model is run with a triangular truncation T199 in the horizontal, and 31 levels in the vertical. The corresponding latitude-longitude quadratic grid has a 0.6° resolution.

Since June 2000, the operational data assimilation system at Météo-France has been a 4D Variational Assimilation usually called 4D-VAR (Rabier et al., 1998). Before it was a 3D Variational assimilation (3D-VAR). These schemes are part of the NWP system developed jointly by ECMWF and Météo-France, see Courtier et al. (1998). The computation of the analysis fields is performed through a global minimisation. In 3D-VAR the minimisation does not include the time evolution of the model, consequently it is much less demanding than 4D-VAR in terms of computer resources. For this impact study a 3D-VAR scheme has been chosen: it is performed every 6 hours: 00, 06, 12 and 18 UTC. A 4D-VAR system would have been necessary for testing the impact of observations reporting frequently, but the TEMP and PILOT observations considered in this study report every 6, 12 or 24 hours. The 3D-VAR system works in “incremental” mode, where the analysis increments are evaluated at T127 for correcting the T199 model. Finally a Digital Filter Initialisation (DFI) is performed after the analysis before running the 96h forecast.

In the control run, all the conventional data are used (surface data including buoys, aircraft reports, radiosondes). The (A)TOVS data (from the NOAA satellites) and the SATOB winds (Atmospheric Motion Winds from geostationary satellites) are also used, but no scatterometer data. In the parallel experimental run, all the radiosonde data are removed, i.e. all the TEMP and PILOT messages, between 20N ans 20S.

---

[1] Service météorologique de Guinée, Conakri, Guinée
[2] Météo France (CNRM), 42 av. G. Coriolis, 31057 Toulouse Cedex, France - philippe.caille@meteo.fr

3. SUMMARY OF THE RESULTS

Comparing the analyses with and without radiosonde data, the biggest differences can be seen on the wind field on the South-East Asia and Australian region mentioned before, where the analysis differences often reach 5 m/s. Outside the tropics the analysis differences are always small, which means that the radiosonde signal does not propagate to mid-latitudes in the data assimilation.

For comparing the forecasts with and without radiosonde data, RMS scores have been computed against the radiosonde observations for different variables, different pressure levels (250, 500 and 850 hPa), and different areas of the globe. Also, for some cases (fig.1), a systematic synoptic evaluation has been performed on the forecast maps, forecast error maps, and forecast differences. The 24h wind score at 500 hPa is almost systematically improved by 0.5 to 1m/s inside the tropics (fig.2): this means that on average the signal coming from the tropical radiosondes is kept for 24h at least. Not much of this positive impact is left at 96h on similar diagrams. However, the signal can occasionally propagate to mid-latitude areas like Asia and affect forecasts up to 96h and up to 50 or 60 degrees of latitude. On one case (runs based on 11 June 2000, 00UTC), the tropical analysis differences on Indonesia and Australia affect a wave pattern moving from China to Kamtchamka. The 96h forecast is improved by the use of tropical radiosondes both on a mid-latitude wave pattern over Japan and on a tropical system inside the tropics (over New-Guinea, fig.1).

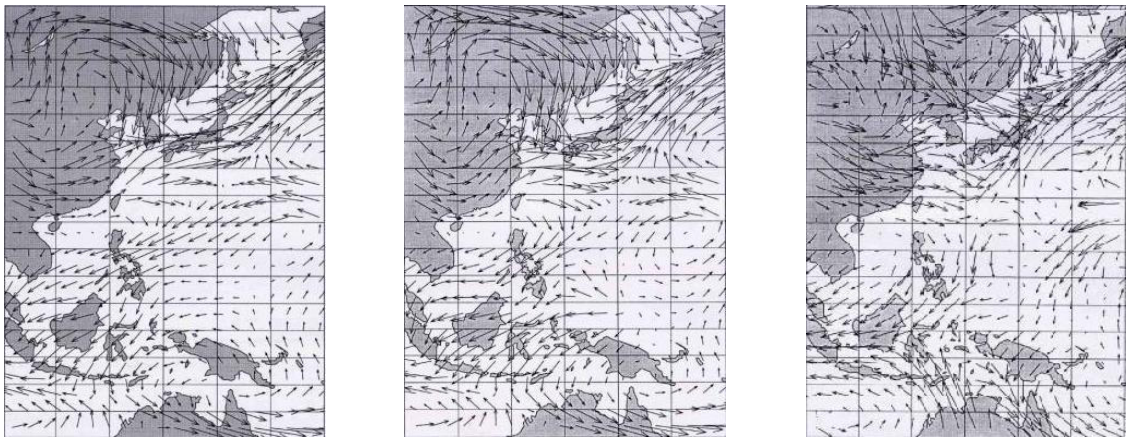

⇧ **figure1** : *an example of positive impact of the tropical radiosondes spreading to high latitudes in the 96h forecast*
250 hPa wind fields from the 96h forecast run from 11 June 2000, 0 UTC, with all the observations (middle), without the tropical radiosondes (left) and from the verification analysis of 15 June 2000, 0 UTC (right).

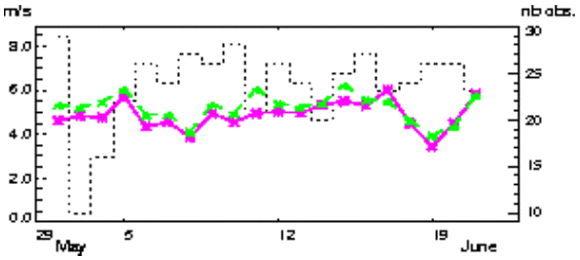

⇦ **figure 2** : *time series of the wind forecast scores computed daily by verification against the radiosonde wind observations. 24h forecast at 500 hPa over the tropical belt (20N-20S).*
The curves are the RMS errors in m/s. The full lines are for the forecast using all the observations, the dashed lines are for the forecasts without tropical radiosonde data. The dotted line is the number of radiosonde wind data used for the verification (vertical scale plotted to the right hand side of the diagram). The verification day is plotted on the horizontal axis (to get the day of the initial state, substract the forecast range).

REFERENCES

♦ Courtier, P., E. Andersson, W. Heckley, J. Pailleux, D. Vasiljevic, M. Hamrud, A. Hollingsworth, F. Rabier and M. Fisher, 1998: The ECMWF implementation of three dimensional variational assimilation (3D-VAR). Part I: Formulation. Q.J.R.M.S.,124, 1783-1807.

♦ Rabier, F., J.N. Thépaut and P. Courtier, 1998: Extended assimilation and forecast experiments with a four-dimensional variational assimilation system. Q. J. R. Meteorol. Soc., 124, 1861-1887.

♦ WMO, 2000: Proceedings of "Second CGC/WMO workshop on the impact of various observing systems on Numerical Weather Prediction". Toulouse, France, 6-8 March 2000. WWW Technical Report 19. WMO/TD N°1034 (available from WMO, Geneva).